buildings

MDPI

Article

Glass-Aluminium Partition Walls with High-Damping Rubber Devices: Seismic Design and Numerical Analyses

Fabrizio Scozzese *, Alessandro Zona and Andrea Dall'Asta

School of Architecture and Design, University of Camerino, Viale della Rimembranza 3, 63100 Ascoli Piceno, Italy; alessandro.zona@unicam.it (A.Z.); andrea.dallasta@unicam.it (A.D.)
* Correspondence: fabrizio.scozzese@unicam.it

Abstract: An innovative solution for aluminium-glass partition walls that can withstand seismic actions without damage is presented. The key feature characterising the proposed innovation is a dissipative coupling between the components of the partition wall, i.e., the glass plates and the surrounding aluminium frame, accomplished through the interposition of high-damping rubber pads (HDRPs). Sliding mechanisms between glass panels and the aluminium frame are permitted through specific detailing solutions, which allow the partition wall to be unsensitive to the inter-storey drift imposed by the hosting structure. A detailed discussion of the system conception is illustrated, showing the main intermediate steps that led to the final solution. The implementation of a refined numerical model is illustrated, and its characteristic parameters are calibrated according to a set of experimental tests previously performed on materials and subcomponents. A numerical application to a case study consisting of a partition wall system installed within a three-storey building is provided to assess the performance of the proposed innovative solution under severe earthquakes.

Keywords: partition walls; non-structural components; floor accelerations; glass-aluminium panels; seismic safety; high-damping rubber; seismic isolation; dissipative coupling; viscoelastic dissipative devices

Citation: Scozzese, F.; Zona, A.; Dall'Asta, A. Glass-Aluminium Partition Walls with High-Damping Rubber Devices: Seismic Design and Numerical Analyses. *Buildings* **2024**, *14*, 2445. https://doi.org/10.3390/buildings14082445

Academic Editor: Hugo Rodrigues

Received: 11 July 2024
Revised: 30 July 2024
Accepted: 5 August 2024
Published: 8 August 2024

1. Introduction

A building is made of structural elements (SEs) and non-structural elements (NSEs). In the former group, there are the parts of the intended load-bearing system (beams, columns, slabs, braces, etc.) that are designed to have adequate capacity against vertical (gravity) and horizontal (wind, seismic) actions. In the latter group, there are those systems not intended to have load-bearing functions, and they can be classified into three categories [1]: architectural components (partitions, parapets, cladding systems, suspended ceilings, etc.), mechanical and electrical equipment (piping systems, power systems, fire protection systems, generators, etc.), and building contents (bookshelves, storage racks, cabinets, other furniture, and decorations).

During a seismic event, even if not intended to be part of the structural system, NSEs interact with SEs, contributing to the global stiffness, strength, and dissipation of the building. Although they are often disregarded in common seismic analysis and design, experimental and numerical simulations indicate that the influence of NSEs on the building seismic response is generally not negligible, both in reinforced concrete (RC) frames, e.g., [2–7], as well as in moment-resisting or braced steel frames, e.g., [8–12]. However, the main concern in seismic design is generally not the influence of NSEs on the structural response but rather the effect that the structural response has on NSEs. In fact, the imposed lateral displacements and inertial forces transmitted to NSEs might cause their damage. Limiting such damage is very important to maintain the building in service, to reduce the likelihood of injury or death, and more in general, to reduce direct and indirect economic losses resulting from earthquakes [13]. It was reported in the technical literature [14,15]

that NSEs comprise most of the investment in commercial buildings and that, among NSEs, partition walls significantly contribute to the total earthquake losses [16–22]. The review of the published technical literature shows that the attention to the seismic performance of partition walls significantly increased in the past decade, focused on two typologies: masonry infills and cold-formed steel-framed gypsum partition walls, the latter often indicated as drywall partitions.

Different innovative proposals for limiting the damage of masonry infills were presented. Preti et al. [23] studied infill walls made of earthen masonry and partitioned with horizontal wooden planks that allow the relative sliding of the partitions, resulting in a high ductility capacity to the in-plane response of the infill and a reduction in its stiffness and strength, hence, minimising damage in the infill when subjected to in-plane loading. Palios et al. [24] proposed bricks not bound together by mortar at bed joints that can slide, leaving the infill panel able to deform freely in its plane, hence, following the seismic motion of the structural RC frame nearly unstressed. Viscous fillers or factory-applied facings can control air, vapor, and water transport via the dry joints, without compromising the movement. Tsantilis and Triantafillou [25] isolated infill panels from the surrounding RC frame using thin layers of cellular materials, significantly preserving the integrity of infill panels at moderate storey drifts and reducing the adverse effects of the infill–frame interaction. Marinković and Butenweg [26] decoupled the RC frame and the masonry infill with a special profile made of elastomeric cellular material. The profile allows relative displacements between the RC frame and the masonry infill and serves, at the same time, as a support for out-of-plane loads. Similarly, Dhir et al. [27,28] proposed the use of masonry infills equipped with rubber joints to absorb most of the in-plane displacement demand of the panel, minimising the stresses induced by the interaction between the panel and the surrounding RC frame.

Compared to masonry infills, better performances can generally be obtained from cold-formed steel-framed gypsum partitions [29–56]. Accordingly, less effort was required to develop innovative solutions to reduce seismic damages, being, in most cases, sufficient to pay more attention to detailing [33], connections [40,41], improvements and strengthening of the aluminium frame [42], activation of friction/sliding dissipative mechanisms [47], sliding and seismic gaps [48,49], and consideration of the influence of boundary conditions in the design [55,56].

Masonry infills and drywalls are not the only available solutions that can be adopted in the subdivision of floors. For example, glass partitions (Figure 1) can be found in office and commercial buildings due to their appealing architectural characteristics. However, the interaction between glass panels (usually thick, and hence, heavy, to meet acoustic isolation needs), their metallic frames, and the structural elements to which they are connected should pose some concerns in case of seismic events, as their failure might endanger life safety and result in high repair and downtime costs. Despite these critical aspects, only a single study can be found in the refereed technical literature, i.e., shake table tests by Petrone et al. [42] on a prototype of a partition with glass panels with improved connections, able to avoid the unhooking of the panels from the supporting studs.

A different approach is followed in the study presented in this paper, where the seismic-resistant capacity of glass-aluminium partitions is obtained by exploiting a passive seismic protection concept inspired by dissipative seismic base isolation systems and scaled to the dimensions of a single module of the partition wall. Such function is assigned to elastomeric elements with viscoelastic properties, capable of creating a dissipative coupling between each glass panel and the perimetral aluminium frame. In this way, it is possible to pursue the objective of seismic safety of the partition without increasing its resistance, thus limiting the dimensions of the aluminium profiles and glass panels as well as avoiding the insertion of bracing or reinforcement systems, both unacceptable in a solution born to be transparent. Specifically, this paper describes the system conception, the structural model implementation and calibration based on experimental tests previously published [57,58],

and the numerical analyses of a realistic case study, illustrated and discussed to assess the potentiality of the proposed innovative solution.

Figure 1. Glass-aluminium partition wall (photograph courtesy of Styloffice S.p.A., Italy).

2. Development of the Design Concept

The development process, from the preliminary ideas to the definition of the solution presented in this study, was characterised by constructive interactions with an industrial producer of glass-aluminium partition walls. Attention was focused on avoiding in-plane damage of the partition wall, while out-of-plane overturning must be contrasted using dedicated connections. Several adjustments and changes were made in the effort to achieve a trade-off between structural efficiency, costs, simple assembly sequences, and aesthetic appeal. The stages of this development process are hereafter presented, describing, in a chronological order, the three main concepts (A, B, and C), and successively highlighting a series of details that were gradually changed and improved.

The glass panels are the same in the three concepts, i.e., transparent stratified glass with a 10 mm thickness (resulting in a mass of 25 kg/m^2 of the in-plane surface), width of 500 mm, and height of 3000 mm. Adjacent panels were connected by means of transparent methacrylate joints attached to the glass through silicon adhesive to produce a continuous partition surface, to avoid pounding between panels, and for the benefit of acoustic isolation.

2.1. Partition Wall Concept "A"

The first concept is schematically shown in Figure 2. The glass panels were kept in their vertical position by means of nylon guides (skids) at their top and bottom ends, allowing in-plane horizontal sliding with reduced friction. High-damping rubber pads (HDRPs) [59–62] were interposed between the top and bottom end sides of the glass panels and the aluminium frame (two pairs of HDRPs at the bottom and two pairs at the top). This solution was simply obtained with the substitution of rigid clamping connections with HDRPs, allowing the use of the same aluminium profiles of commercially available partitions of the same typology. However, this solution was disregarded after extensive numerical simulations because it did not allow the uncoupling of the partition wall from the

top floor, leaving the system drift sensitive, hence with consequent difficulties in achieving a controlled deformability of the glass panels.

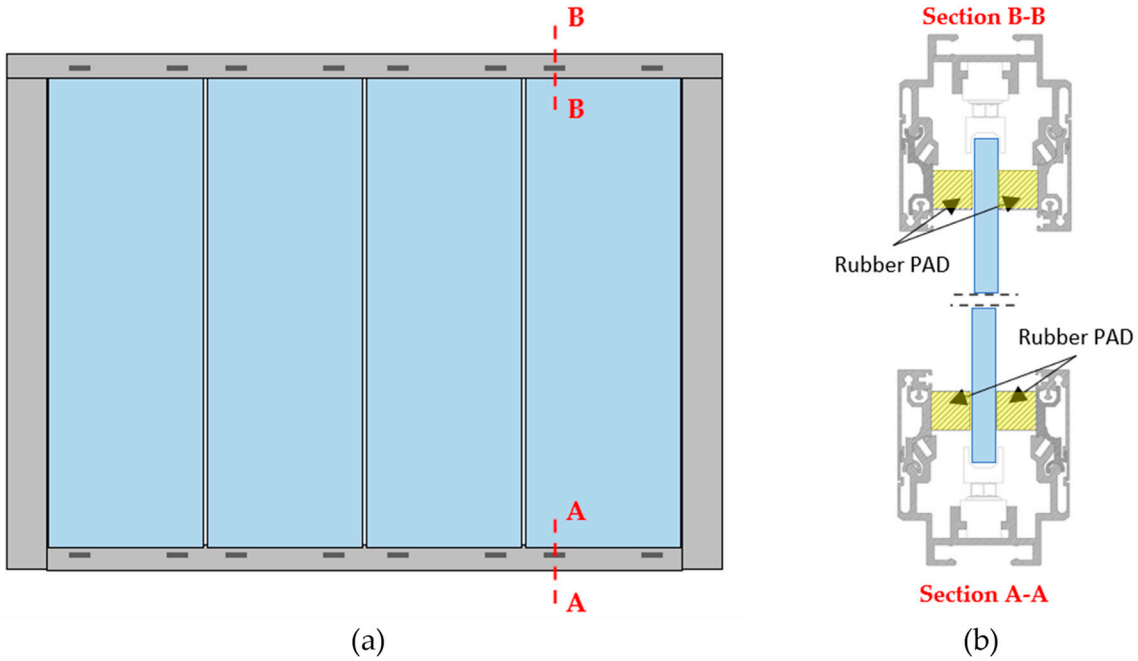

Figure 2. (**a**) First conceptual scheme, with rubber pads placed both at the top and bottom of the portal frame. (**b**) Related cross-sections.

2.2. Partition Wall Concept "B"

The initial proposal was revised and evolved into a second concept (Figure 3). Changes were made in the upper frame profile, which constituted two independent components that were supposed to slide one over the other along their longitudinal axis with negligible friction (levigated and lubricated interacting surfaces). The outer part was intended to be connected to the ceiling of the hosting building, while the inner part clamped the glass panels. The rubber pads were placed at the bottom interface only (Figure 3b). Accordingly, with less pads required, the design of a sufficiently small horizontal stiffness was easier, allowing to find solutions compatible with available HDRPs. However, concept "B" was not fully convincing due to the uncertainties related to the actual friction force that could arise between the outer and inner top aluminium profiles, as well as to aesthetic problems following their larger dimensions.

2.3. Partition Wall Concept "C" (Final)

The third and final solution is presented in Figure 4, where the top part of the aluminium frame was simplified using a profile clamping the glass panel that was allowed to horizontally slide along a guide through low-friction skids. A more detailed representation is provided in Figure 5, where the components are numbered for their clear identification in the discussion of their roles.

Three different arrangements of the same aluminium profile (4) are used in the bottom, top, and lateral sides of the frame. The discussion of the geometry and functions of such arrangements follows below.

The upper horizontal profile (Figure 5b) connects the partition to the intrados of the upper floor, directly to the structural elements or through the suspended ceiling, depending on the architectural features of the building. A C-shaped profile (5) is fixed to the upper floor intrados or ceiling and housing skids (3) made of low-friction material. They act together as sliding guides along the horizontal in-plane direction for the profile (4), which in turn fasten the glass panels (9) through a set of arms (7), at least two pairs every single

panel. The arms (7) exploit spacers (6) to connect the panels (9) to the profile (4), exerting the function of out-of-plane restraint for the glass (9). A pair of covers (8) was added for protection and aesthetic functions. It is worth noting that the profile (4) was shaped to grant space for vertical movements of the glass panels, beneficial to avoid locking of the panels in case of severe seismic events when damage in the structural elements could induce deformations on the aluminium frame, but also in the installation process to allow an easy placement of the glass panel in its correct position.

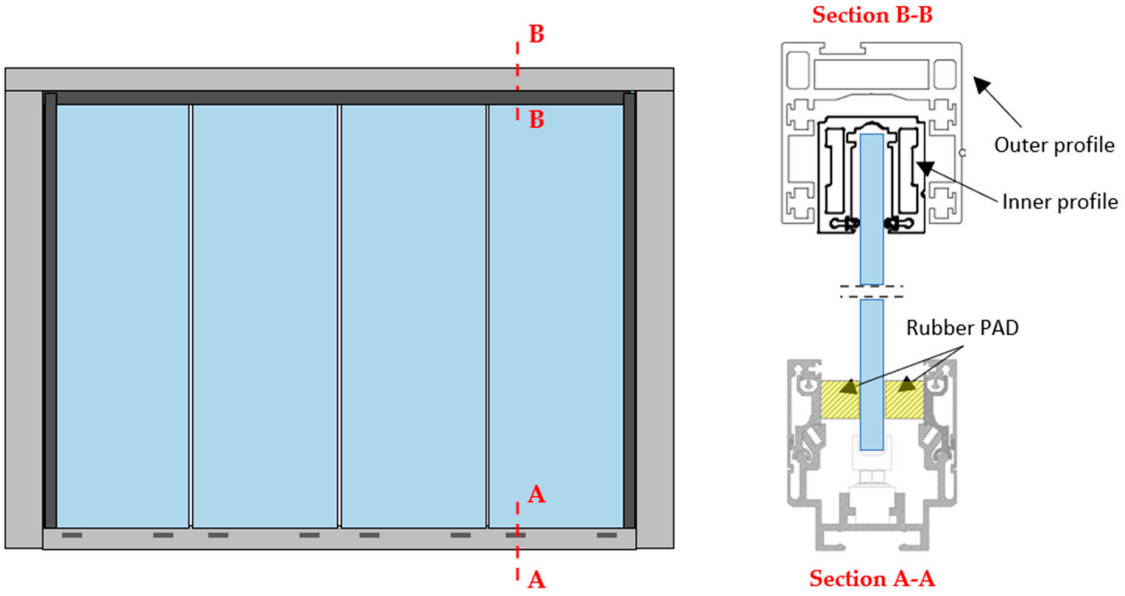

Figure 3. (**a**) Second conceptual scheme characterised by the presence at the top of inner and outer aluminium portal frames, while rubber pads were placed only at the bottom. (**b**) Related cross-sections.

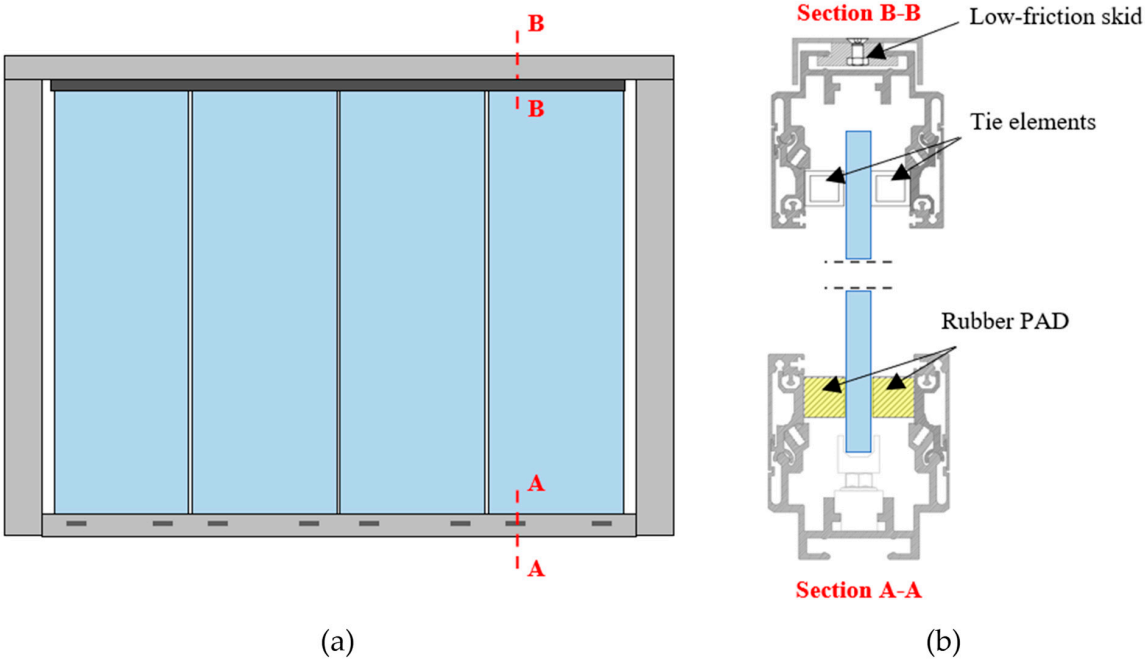

Figure 4. (**a**) Third conceptual scheme characterised by the presence at the top of a sliding aluminium portal frame and rubber pads placed only at the bottom. (**b**) Related cross-sections.

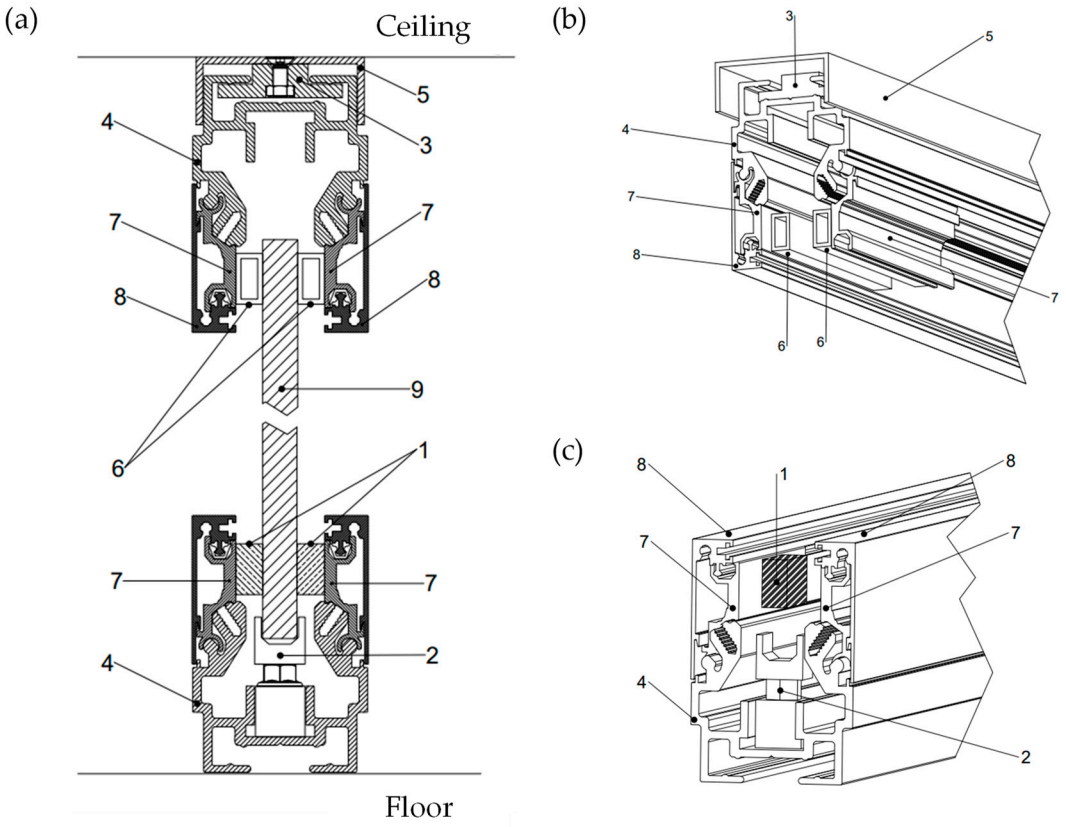

Figure 5. Glass-aluminium partition wall, structural details with numbered system components: (**a**) cross-section, (**b**) axonometric scheme of the upper profile, and (**c**) axonometric scheme of the bottom profile.

The lower profile (4; Figure 5c) is rigidly fixed to the floor. A set of arms (7) realises the connection between glass plates (9) and aluminium profiles (4), through HDRPs (1) creating a dissipative coupling by exploiting the damping properties of the rubber. The floor profile (4) also houses height-adjustable skids (2), having the two-fold aim of levelling the glass panels (adapting to the specific floor conditions and imperfections) and bearing the panel self-weight. The skids (2) were made of low-friction materials to allow the panels to slide horizontally. Thus, the skids (2) of the lower profile and the skids (3) of the upper profile, together, allow the in-plane motion of the glass plates required to activate the shear deformation of the HDRPs (1). Again, a pair of covers (8) was added for protection and aesthetic functions.

The lateral vertical profiles (Figure 6) are geometrically identical to the lower profile, except for the HDRPs, which were replaced by spacers having the same thickness of the pads but realised with a low-friction material. Hence, the in-plane sliding of the glass panels is allowed, while the transversal out-of-plane movements are opposed. These vertical profiles could be self-standing or bounded to the building structural elements, e.g., structural walls or columns. In either case, the profile grants space for the lateral movement of the glass (clearance of 25 mm), larger than the predicted maximum stroke as a safety margin to prevent pounding under dynamic actions (see Figure 6a). Similarly, tolerances (20 mm) were left on the top between the glass panel and the floor profile (4) to accommodate vertical movements of the glass panels produced by the rocking or other unexpected actions.

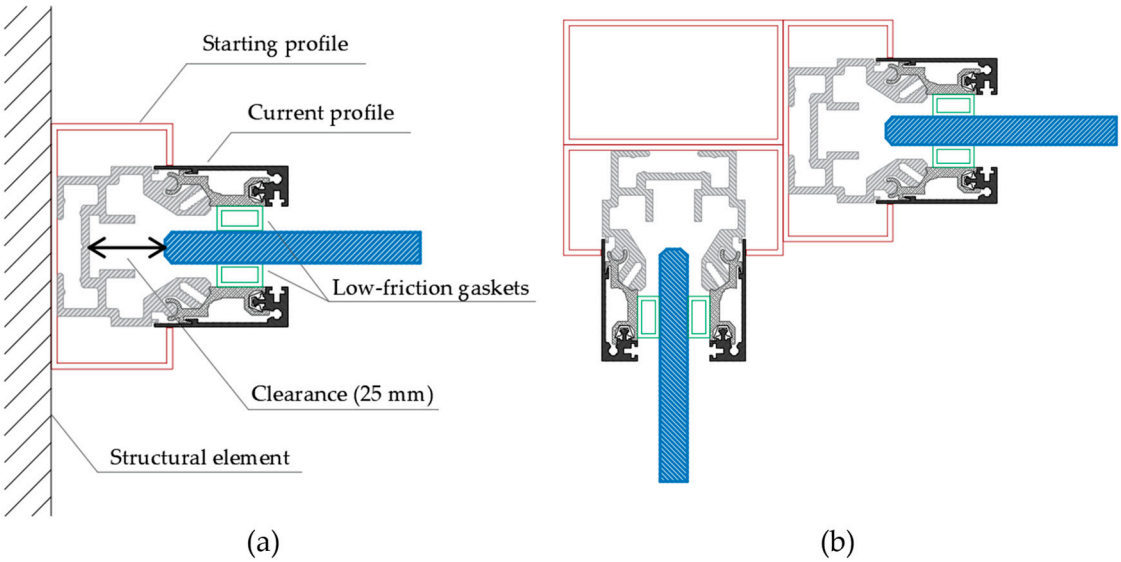

Figure 6. Vertical profile cross-sections: (**a**) connected to a structural element and (**b**) corner self-standing solution.

It is worth noting that the surrounding aluminium portal frame was conceived to have screwed connections with negligible rotational stiffness between its vertical and horizontal components (almost pinned connections). In this way, the bending moment in the frame elements is limited; accordingly, no flexural damages are expected on these elements. With the considered details and tolerances, the system is expected to work effectively in any location (within both seismic-resistant and gravity-resistant portal frames) and remain operational for ordinary conditions of installation, hence also in case of deflections of the floor. However, it should be considered that situations where very severe deformation occurs in the structural elements, representative of near-collapse conditions, do not represent the reference scenario for the validation of the proposed solution. In such conditions, the preservation of non-structural elements (such as partition walls) could not be a reasonable objective of the seismic design. Nevertheless, the considered design for the proposed partition wall should allow its survival up to very large structural damages, thanks to the space allowed for the glass panel movements with respect to the aluminium frame, as already discussed. Moreover, the risk of problems and damages in case of significant structural deformation might be mitigated by connecting the top of the wall to the ceiling, avoiding a direct connection to the upper floor.

3. Seismic Design and Detailing

3.1. Analysis of the Dissipative Mechanisms

The proposed final concept allows uncoupling the mass of the partition wall (almost totally contributed by the glass panels) from the building inter-storey response, making its in-plane response dependent only on the acceleration of the floor on which it was installed. In case of seismic events, the glass panels can move in their plane (Figure 7), and this motion produces shear strains on the rubber pads (Figure 8) that dissipate kinetic energy thanks to their high-damping properties.

The movement of the panels is the superposition of a primary translational mechanism and a secondary rotational mechanism. The horizontal translational movement of the glass panels (Figure 7a) was intended to be the main source of energy dissipation of the proposed system. Accordingly, this was the mechanism considered in the design of the HDRPs. The secondary dissipative mechanism takes place at the interfaces between adjacent glass panels, where the methacrylate joints can be deformed due to minor in-plane rotational (rocking) movements (Figure 7b) caused during a seismic event by the fact that the upper and lower restraints are not perfect sliders, and amplified by the geometry of the panels,

which are high and narrow. Such rotational movements were not considered in the design, although the numerical model was made to include their contribution in the seismic response of the proposed partition wall. Vertical translations, such as those determined by the glass panel uplift in the case of upward vertical accelerations larger than gravity, were also not explicitly considered in this design stage, as they are very unlikely to occur in the seismic hazard scenario assumed in this study. Nevertheless, as already mentioned in the previous paragraph, there is large clearance to accommodate vertical movements of the glass panels. It shall be also noted that the HDRPs, although engaged in their weak axis, would likewise be activated to dissipate the vertical kinetic energy.

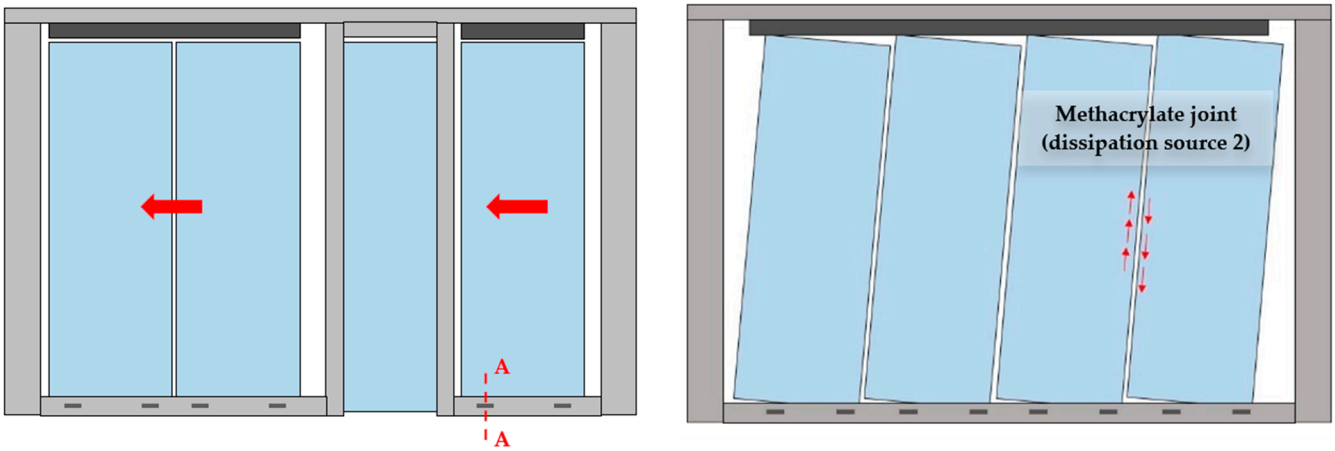

Figure 7. Schematic representation of two independent mechanisms in the glass panels contributing to their in-plane motion: (**a**) horizontal translation (red horizontal arrows) and (**b**) rotation (rocking) with red arrows indicating part of the interaction forces induced in the methacrylate joint.

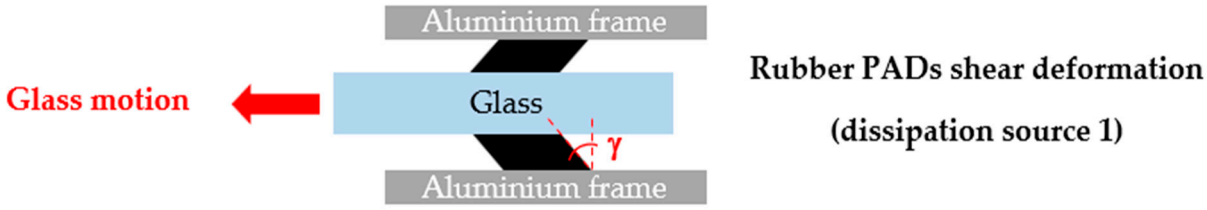

Figure 8. Schematic detail of the rubber pads' deformation induced by the glass in-plane motion (cross-section A-A of Figure 7a).

3.2. Detailing of Partition Components

3.2.1. Sliding Supports

As already mentioned, the height-adjustable skids play both a functional and structural role in the proposed system. The former consists in the possibility of adjusting the height to guarantee the levelling of the partition wall even on floors that are not perfectly flat. The structural role is that of vertical support of the glass panels, i.e., the feet shall transmit the vertical loads without restraining the translational motion of the glass inside the bottom aluminium frame, and this was made possible using specifically designed elements made of low-friction materials (for example, Nylon was used in the first prototypes) with a contact surface as small as possible. To achieve these requirements, the skid was modified from its preliminary shape (Figure 9a) to a final version (Figure 9b), where the geometry was also changed to increase the stability against overturning. In Figure 9c, a three-dimensional view of the base profile with its main components is provided. The alignment of the sliding supports is guaranteed by a rail positioned centrally at the base of the profile, as illustrated

in Figure 10, showing some physical prototypes made as proof of concept during the intermediate stages of the design concept development.

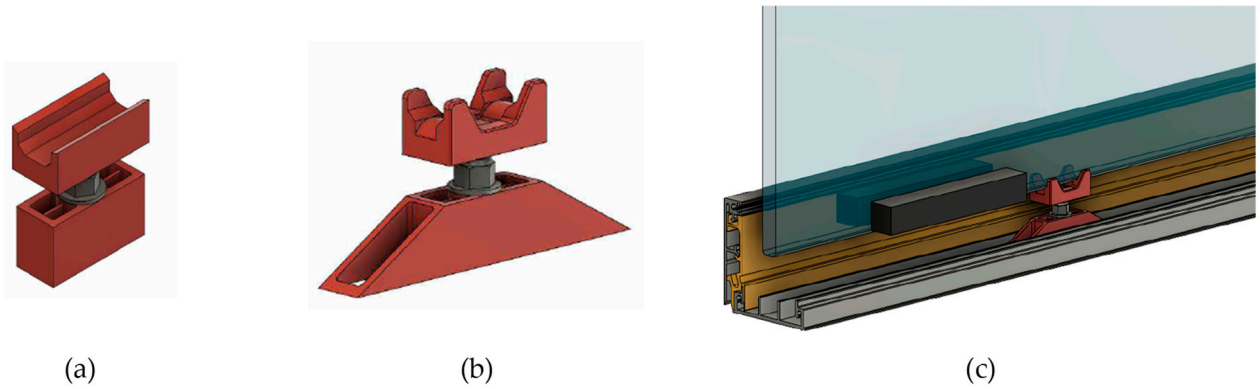

(a) (b) (c)

Figure 9. Sliding supports for the glass plates: (**a**) preliminary and (**b**) refined versions. (**c**) A 3D render of the base profile with its main components.

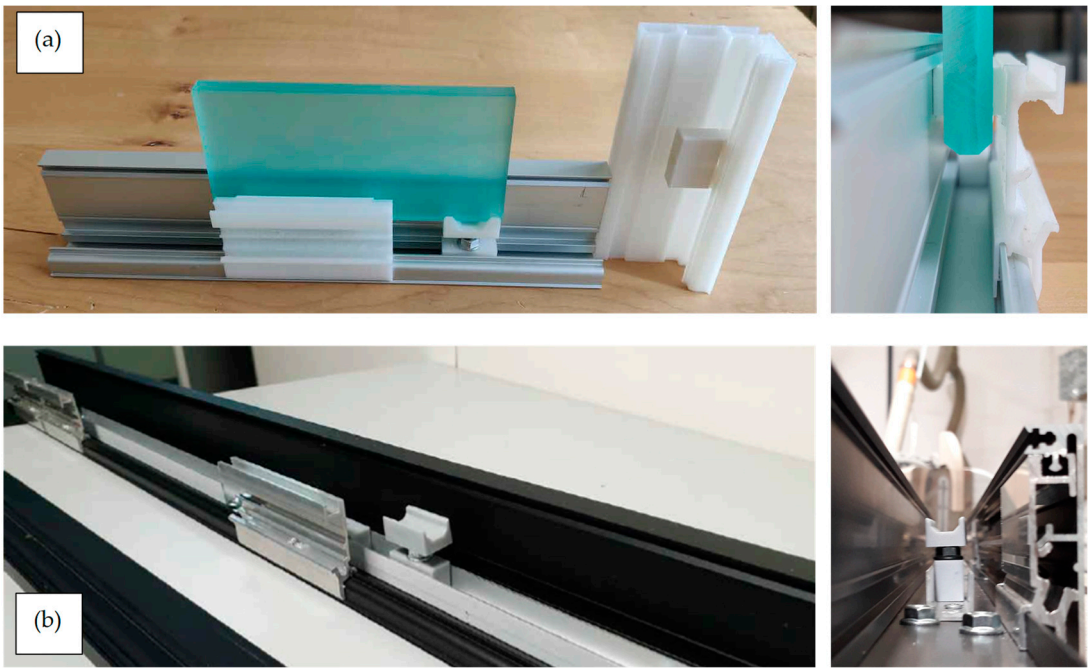

Figure 10. First prototypes developed as proof of concept during the intermediate stages of the project: (**a**) preliminary concept with 3D-printed elements and (**b**) preliminary aluminium prototypes.

3.2.2. Rubber Compounds for the Dissipative Pads

The rubber pads represent the key elements of the proposed innovative solution and, as with every other aspect of the proposed system, evolutionary steps were performed before converging to the final solution. The first trial was carried out adopting a recycled rubber compound made by a producer specialised in acoustic isolation and vibration damping. Unfortunately, the recycled material was revealed to be inadequate for the purposes of the proposed partition, as highlighted during preliminary experimental tests performed on some of the samples shown in Figure 11a, due to the following reasons:

- Premature crisis of the pads was observed at maximum shear strain, γ, equal to 0.7–0.8, i.e., displacement equal to 70–80% of the rubber thickness.
- Impossibility to reduce the thickness of the pads below 15 mm, with repercussions on the dimensions of the profiles that would negatively impact the aesthetic value.

(a) (b)

Figure 11. Rubber samples provided by two different manufacturers: (**a**) recycled rubber and (**b**) high-damping rubber.

Accordingly, the authors chose to use high-damping rubber (HDR), commonly used for seismic isolators and produced by specialised industrial manufacturers, which consists of compounds with added filler [63] to achieve highly dissipative properties, i.e., a supplemental damping $\xi > 10\%$.

Differences between the two compounds were noticeable, as outlined below:

- From visual comparison (Figure 11), it can be noticed how the HDR compound is homogeneous, while the recycled rubber not (larger grain).
- The HDR compound is considerably stiffer than the recycled rubber, as illustrated in Figure 12a, where the shear modulus function, $G(\gamma)$, is reported, and this allowed to notably reduce the thickness of the pads below 10 mm, leading to benefits in terms of aluminium profile dimensions.
- Figure 12b shows a comparison between the damping properties of the recycled rubber compound and the HDR compound. It is worth noting that the recycled rubber has negligible dissipative properties for shear strain lower than 0.5, while a larger dissipation was observed for shear strain $\gamma > 0.5$ as a consequence of the progressive damage and relevant post-failure friction mechanisms. The damping ratios of the HDR compound are almost two times higher than those of the recycled rubber, and the values remain roughly constant with γ (see $\xi(\gamma)$ in Figure 12b), with major gains in terms of seismic energy dissipation.
- The strain capacity of the HDR compound is notably greater than the recycled rubber capacity ($\gamma < 0.8$). This provided prominent advantages from the point of view of the system safety in case of future extreme events larger than the design ones.

The differences in stiffness of the two rubber types notably influenced the pad geometry following from the seismic design: the stiffer the rubber, the shorter the pad. Moreover, the available maximum shear strain value affected the choice of the thickness: the recycled rubber, due to its limited deformability, needs a higher thickness to attain a given target displacement. A physical comparison between pads of recycled rubber and HDR satisfying the same design criteria is provided in Figure 13.

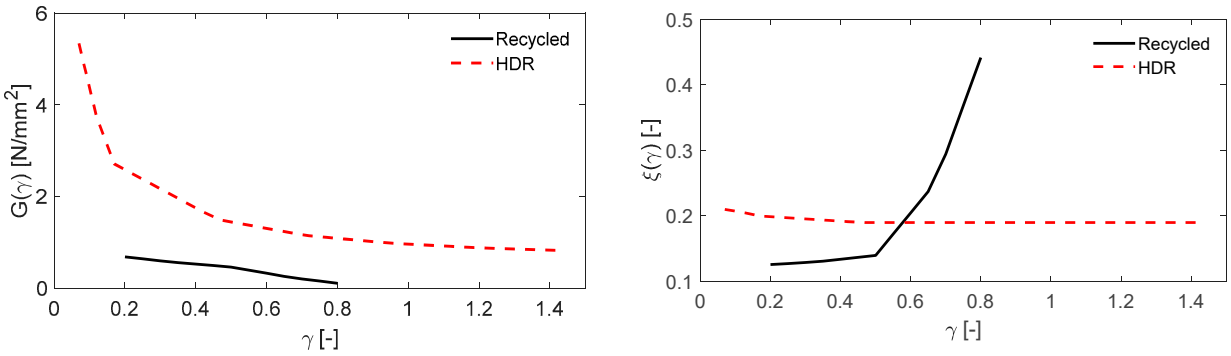

Figure 12. Comparison between recycled rubber and HDR (data provided by the producer): (**a**) shear stiffness and (**b**) damping ratio vs. shear strains.

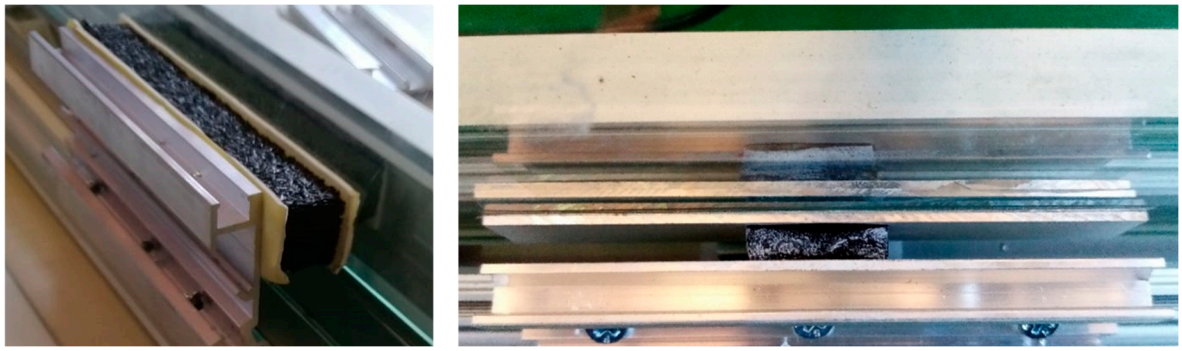

Figure 13. (**a**) Recycled rubber pad (H × W × L = 15 × 15 × 150 mm^3) simply connected through bi-adhesive tape and (**b**) HDR pad (H × W × L = 6 × 8 × 20 mm^3) glued with intermediate aluminium plates.

To verify that the HDR properties were stable under different working conditions (this might not always be the case with viscoelastic dampers [64–66]), characterisation of HDRPs was performed directly by the producer with sinusoidal cyclic tests at 1 Hz and 5.0 Hz frequencies, thus, covering the expected frequency range in the case of seismic events, such as those considered here. The results are shown in Figure 14, where the scarce sensitivity of the HDR within the range of strain velocity of interest is confirmed [61,67].

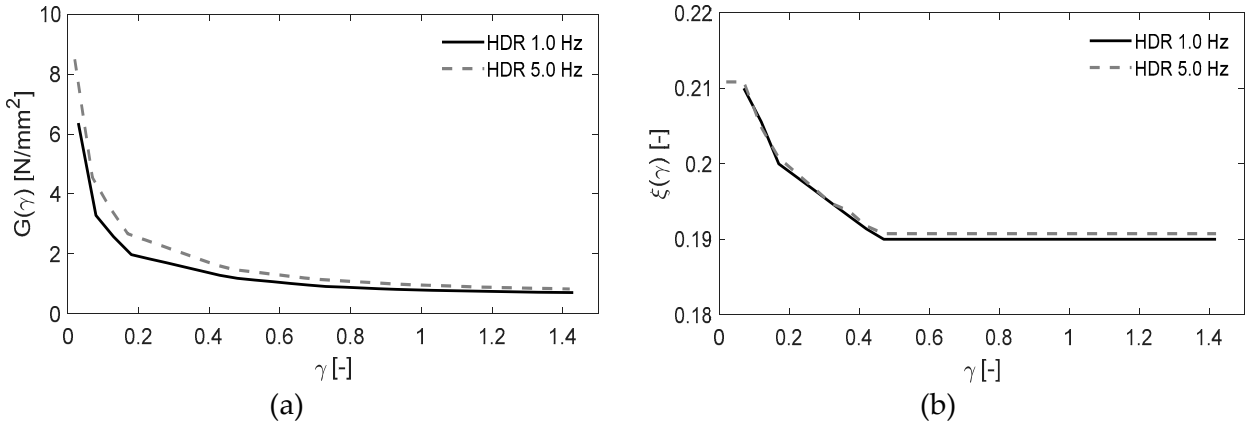

Figure 14. Effect of testing load frequencies in the HDRP: (**a**) shear stiffness and (**b**) damping ratio vs. shear strains (data provided by the producer).

It is worth noting that the HDRPs were not tested for their axial through-the-thickness properties. However, due to their very limited thickness (6 mm) and being rigidly connected to the aluminium horizontal profiles (see element (7)), HDRPs worked as restraints for the out-of-plane horizontal displacement, while providing a negligible degree of restraint for the out-of-plane rotations. Hence, HDRPs are expected to behave as cylindrical hinges for the out-of-plane movements.

3.2.3. Panel–Pad–Frame Connections

Connections between glass panels, pads, and the aluminium frame are critical aspects for the system to perform as intended. It is very important to ensure over-resistant connections to allow the deformation of the pads during seismic events. Several connection methods were studied, some of which were also tested, while others remained only hypotheses. Among the solutions experimentally investigated were the following:

- Adhesive connection via Tesa 64,958 double-sided tape, which revealed poor results in connecting rubber interfaces (surface was too small) but turned out to be good for aluminium–aluminium and aluminium–glass connections.
- Glued connection, where the use of universal glue (Bostik) and cyanoacrylate super-glue (Loctite 480) was investigated. The cyanoacrylate super-glue proved to have very high adhesive performances to connect aluminium–rubber interfaces, while performance notably reduced on rubber–glass interfaces.
- Accordingly, the following mixed connection was proposed (Figure 13b): a small rectangular aluminium plate was interposed between the glass panel and the rubber pad; the glass-to-aluminium interface was connected via double-sided adhesive tape; the rubber-to-aluminium interface was glued via cyanoacrylate super-glue; on the external side of the profile, i.e., between the pad and aluminium arms (see element 7 in Figure 5), a glued connection was adopted.
- Among the connections that were conceptualised but not tested, one with a potential practical interest is reported in Figure 15, which consisted of an ad-hoc opening on the glass panel, realised to house the rubber pads within it. This solution would eliminate the need for a glued interface between HDR and glass; however, it requires further work on the glass panels to make the necessary holes.

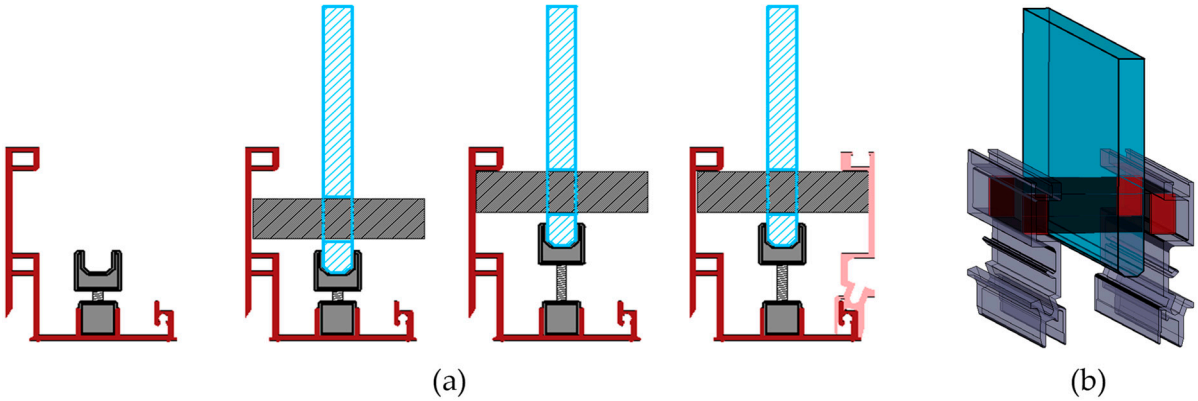

Figure 15. Alternative panel–pad–frame connection strategy requiring an ad-hoc opening on the glass plates for pad housing: (**a**) scheme of the installation sequence and (**b**) three-dimensional view.

4. Numerical Model Definition and Calibration

Experimental results of the subcomponents, reported in [57,58], were exploited to calibrate a finite element model of the partition wall, implemented in the software SAP2000 Ultimate V25.3 [68], for numerical validation of the proposed system. This section is organised as follows: first, the calibration of the models for the two main energy dissipation sources (pads and methacrylate joints) are presented; afterwards, the model of a small-scale prototype subject to shaking motions is reported.

4.1. Rubber Pad Modelling

An equivalent linear viscoelastic model was adopted [69,70]; therefore, following a constitutive law governed by two parameters (Equation (1)): the effective stiffness, $k_{eff}(\gamma)$, and the equivalent viscous coefficient, $c_{eq}(\xi, \gamma)$ (ξ = damping ratio, and γ = rubber shear strain):

$$F(x, \dot{x}) = k_{eff}(\gamma)x + c_{eq}(\gamma, \xi)\dot{x}, \quad (1)$$

where F is the resisting force, x is the displacement, $\dot{x}$ is the velocity, and ξ is the rubber damping ratio (depending on γ). The calibration was carried out by numerically simulating the experimental cyclic dynamic tests performed under a set of sinusoidal inputs with a frequency of 1 Hz and increasing amplitudes (D = 2.5, 5.0, and 7.5 mm). Table 1 summarises the parameters of the calibration carried out in accordance with FEMA 274 [71] at the different maximum displacements. The viscoelastic modelling of the rubber was found to be adequate, as testified by the almost perfect overlap of the numerical hysteresis cycles with the experimental ones (Figure 16).

Table 1. Viscoelastic parameters of the rubber pads calibrated based on the experimental tests.

γ_{max} (-)	D (mm)	k_{eff} (N/mm)	ξ_{eff} (-)	C_{eq} (Ns/mm)
0.17	2.5	145.00	0.12	5.54
0.33	5.0	116.00	0.13	4.62
0.50	7.5	86.00	0.14	3.83

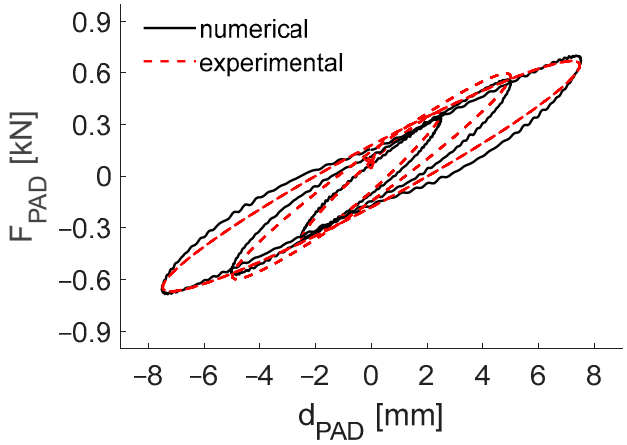

Figure 16. Comparison between numerical and experimental hysteresis loops of rubber pads.

4.2. Methacrylate Joint Modelling

As already mentioned, vertical joints in methacrylate with an interposed silicon film were placed between adjacent glass panels. According to the experimental results, this interface showed a viscoelastic behaviour with good dissipative capacity, activated by the relative sliding between the glass panels. As in the pad modelling, an equivalent viscoelastic model was used:

$$F(x, \dot{x}) = k_{eff}x + c_{eq}|\dot{x}|^{\alpha}\mathrm{sgn}(\dot{x}), \quad (2)$$

where the parameter α regulates the nonlinearity of the response with the velocity and sgn(•) is the sign operator. The calibrated model parameters are reported in Table 2 for experimental tests performed with two different frequencies: 1 Hz and 2 Hz. The comparison between numerical and experimental responses is reported in Figure 17, which shows how simple linear (α = 1.0) models can reasonably reproduce the experiments.

Table 2. Viscoelastic parameters of the methacrylate joint calibrated based on experimental tests.

Frequency (Hz)	k_{eff} (N/mm)	C_{eq} (Ns/mm)	α (-)
1.0	80.0	18.0	1.0
2.0	90.0	12.0	1.0

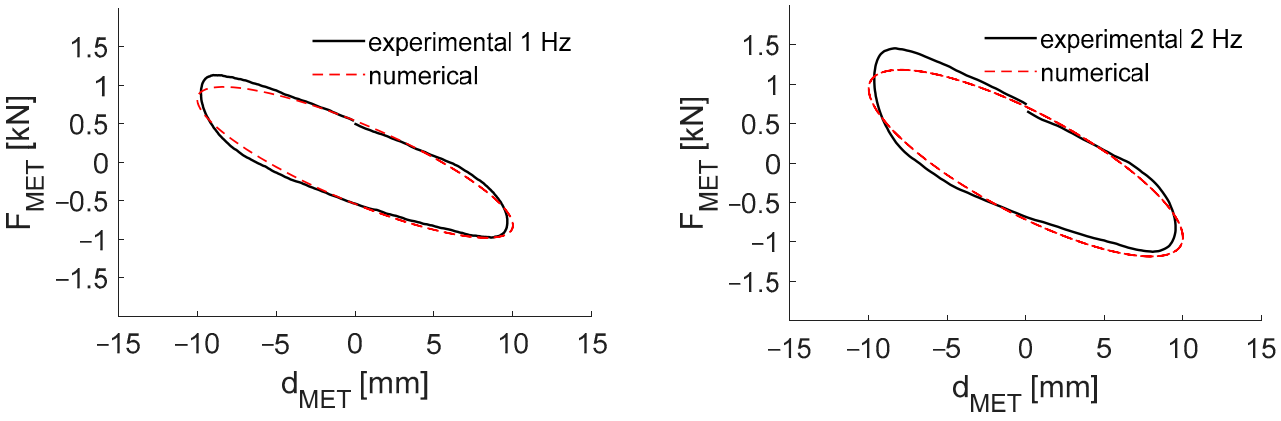

Figure 17. Comparison of numerical and experimental hysteresis loops of the methacrylate joint.

4.3. Small-Scale Experimental Test Modelling

After the characterisation of the materials and subcomponents, a small-scale assembly of the partition wall was tested under imposed cyclic horizontal displacements, as illustrated in [57,58]. The prototype consisted of two glass plates with an interposed vertical methacrylate joint, two pairs of pads plus two pairs of sliding supporting skids at the base of each glass panel, and two horizontal rigid rods hinged at the panels and at the contrast frame. The prototype tests were modelled in SAP2000 Ultimate (Figure 18). The following assumptions were made in the definition of the implemented finite element model:

- Rubber pads at the wall base were modelled as viscoelastic links, with equivalent properties calibrated, at proper shear strain levels, γ, based on the results of the mechanical laboratory characterisation.
- The methacrylate joint response was modelled by a set of viscoelastic links connecting the adjacent panels and activated by their relative sliding motion (properties derived from experimental tests).
- Sliding skids were inserted at the base of each panel and modelled through link elements (two links per glass panel) with elastoplastic behaviour along the horizontal direction, accounting for the low-friction property (Fmax = 50 N) and having a unilateral constraint property along the vertical direction, i.e., a gap element was adopted to allow contact in compression only, with the possibility of traction detachment of panels from the base supports.
- Each glass plate was individually modelled as an elastic thin shell (10 mm thick) with a distributed mass of 25 kg/m^2.

The comparisons between the numerical and experimental responses are provided in Figure 19 for a sinusoidal input (1 Hz frequency, 3 cycles, with amplitude 10 mm) in terms of the (a) total force–displacement hysteresis curve and (b) friction force–displacement cycles. The average displacement at the base of the two glass plates (see d_1 and d_2 in Figure 18b) was considered in the plots. The comparison highlighted a quite satisfactory match between the test and the model (less than 7% overestimation of the glass displacements). It is worth noting, moreover, that the same test was repeated using different input frequencies, and the same trend of the force–displacement diagram was always observed, therefore excluding the dependence on the test frequency of the stiffness and dissipative capacity of the experimental model. This outcome positively reflects on the reliability level of the numerical model.

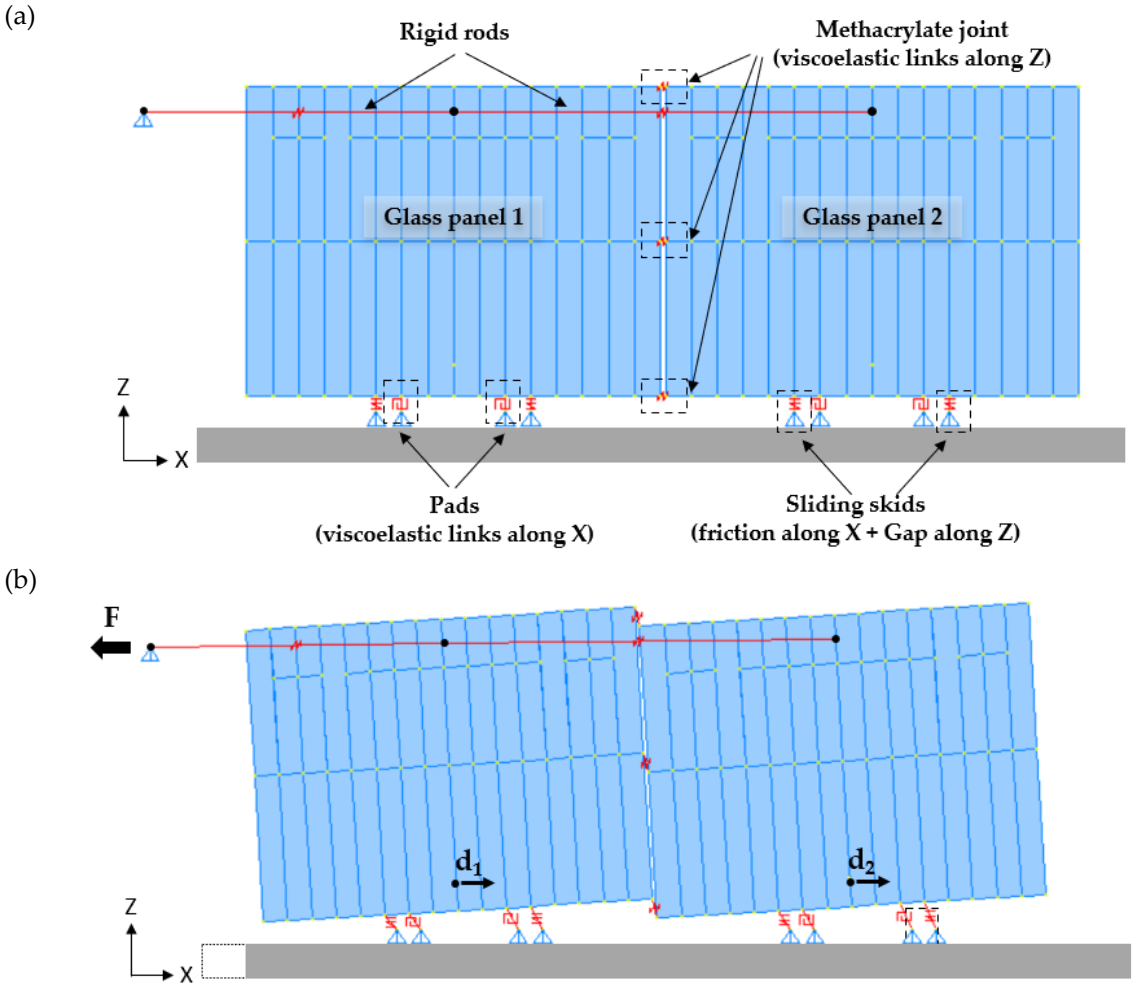

Figure 18. Numerical model of the small-scale partition wall: (**a**) system at rest, with components highlighted, and (**b**) system kinematic response during the simulation.

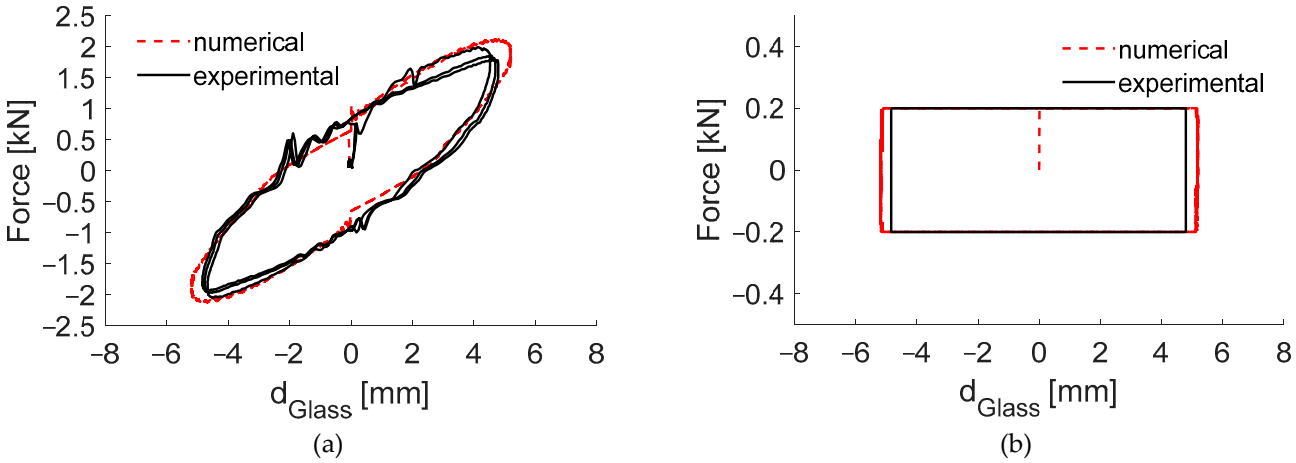

Figure 19. Comparison between numerical and experimental responses of a small-scale assembled partition wall: (**a**) total force–displacement hysteresis curve and (**b**) friction force–displacement cycles.

5. Seismic Performances of the Proposed Dissipative Partition Wall within a Building

5.1. Case Study Description

This section illustrates the outcomes of a numerical application performed to show how the proposed system behaves within a realistic scenario. The building used as a case study is a three-storey reinforced concrete building built in Italy in the 1980s (Figure 20). The inter-storey height is 4.0 m, and the beam span ranges between 5.7 m and 7.0 m. The whole building is composed of four structural blocks, separated by structural joints sufficiently wide to consider each system dynamically independent from the others. One of the portions of the building was considered in this study, and a numerical model was developed, where beams and columns were implemented as elastic frame elements, rigid floor constraints were inserted at each storey level (the floor structural typology and features justified this assumption), and restraints were fixed at the ground level.

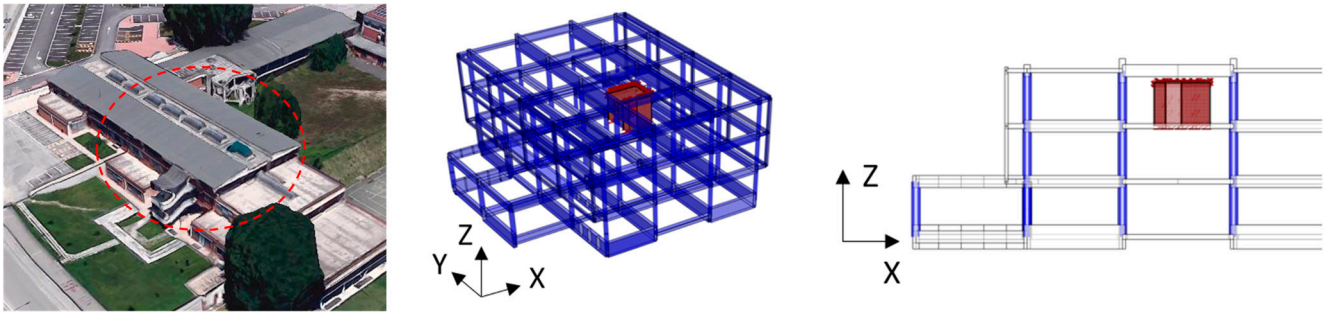

Figure 20. Case study building and numerical model: (**a**) aerial view with the considered portion marked with a dashed red circle, (**b**) three-dimensional finite element model, and (**c**) vertical section with the considered partition wall.

It was assumed that the third level of the building hosts a partition wall with a horizontal C-shaped configuration made by three walls, one equipped with a door, as in Figure 21 (geometrical schemes) and Figure 22 (numerical model). The geometrical dimensions are length (along X) = 3.54 m, width = 3.00 m, and height = 2.70 m. The lower and upper profiles are rigidly connected to the floor and ceiling, respectively. The self-weight and mass of all elements were accounted for, even if the major part was contributed by the glass panels only.

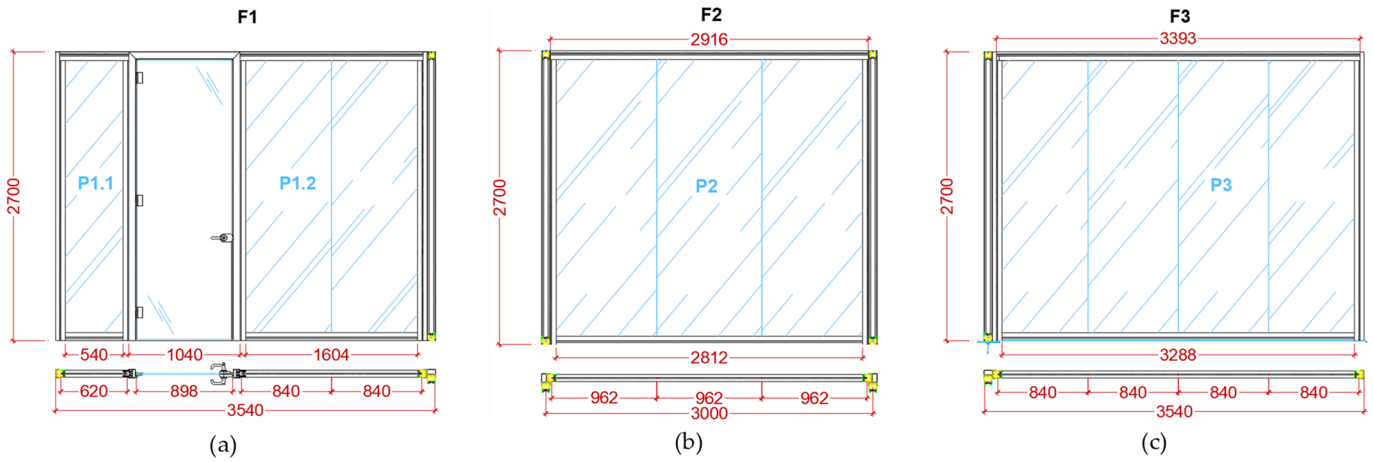

Figure 21. Geometrical details of the three panel-assembly facades: (**a**) F1 (glass panels P1.1 and P1.2), (**b**) F2 (glass panel P2), and (**c**) F3 (glass panel P3).

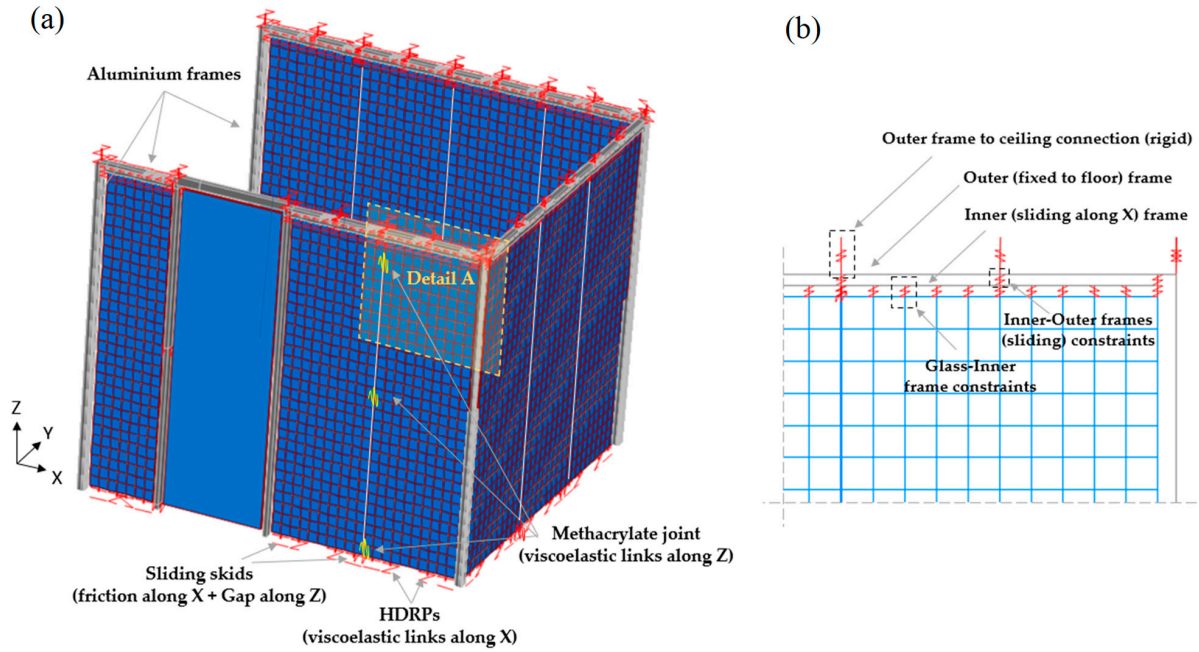

Figure 22. Numerical model of glass-aluminium partition wall assembly: (**a**) model overview and (**b**) detail of the top connections (close-up of Detail A indicated in (**a**)).

5.2. Seismic Input

The seismic hazard considered in this case study is representative of a medium–high seismicity area in Italy, characterised by a peak ground acceleration (PGA) of 0.35 g at the Life Safety Limit State (with a return period of 475 years). A set of 10 recorded ground motion time series was selected from the European Strong Motion Database (ESD) and scaled to better reflect the hazard intensity of the considered scenario. The selected ground motions and related acceleration response spectra are provided in Figure 23, where a different colour is used to represent each earthquake sample (the same colours used for the accelerograms were adopted for the related spectra). In Figure 23b, both the average and target spectra are also reported to highlight the fulfilment of the spectrum-compatibility condition.

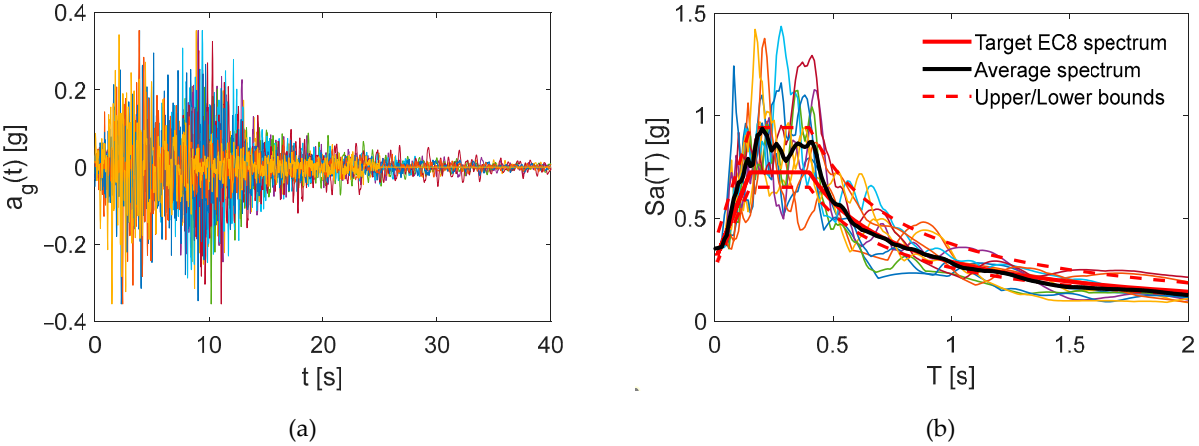

Figure 23. (**a**) Ground motion samples conditional to a hazard level consistent with the Life Safety Limit State (475-year return period) and (**b**) related response spectra.

5.3. Design of HDRPs

The design of the pads was carried out by considering a single degree of freedom (SDOF) system, having the mass of a single glass panel (length 840 mm, height 2700 mm, and thickness 10 mm) and the stiffness and damping provided by two pairs of pads. The

design process was carried out by adopting an average displacement response spectrum and proceeding iteratively with the same process adopted for the design of seismic isolators [62], changing the geometry of the pads until convergence between spectral demand and shear deformation was achieved. The difference is that in this case of dissipative partition walls, the fundamental period and the level of deformation were much lower, as compared to isolated buildings, i.e., displacements were of the order of a few centimetres and the fundamental period was around 0.20 s.

Considering the seismic scenario described above and following the design approach just delineated, the resulting pads were parallelepipeds, with $H \times W \times L = 6 \times 8 \times 20$ mm^3 (an example is provided in Figure 13b). One single size of pads was used for the whole assembly, and the number of pads was accordingly determined in proportion to the masses of the glass panels. It is worth noting that the possibility to choose the number of pads for each glass panel makes the system easily adaptable to a given seismic hazard condition of the site and/or to the specific floor of the building in which the partition wall is installed.

5.4. Numerical Simulations and Performance Evaluation

The finite element model presented in the previous Section 5.1 was used to run ten nonlinear dynamic time history analyses, exploiting the set of ground motion samples introduced above. Analyses were unidirectional, performed along the X direction only, and allowed studying both the in-plane and out-of-plane behaviours thanks to the considered geometry. Each seismic analysis was preceded by an incremental gravity analysis accounting for the self-weight of all components of the partition wall, as previously illustrated.

The following selection of response parameters was used to characterise the dynamic behaviour of the system: relative displacements (see the scheme in Figure 24) between the glass and the portal frame (Δ_1 and Δ_2) in order to assess the sufficiency of the glass end-stroke and, thus, the safety margin against an impact among components; the drift of the aluminium portal frame (δ_F) and the drift of the glass plates (δ_G), with the former also being representative of the building inter-storey, while the latter providing insight about the entity of the rocking motion of the panels; maximum stresses on glass plates (in particular on F2 of the box experiencing a bending stress out of its plain) and on aluminium frames. These quantities were monitored for each group of glass panels (according to the numbering of Figure 22): panels P1.1 and P1.2 of facade F1, P2 of F2 (orthogonal to the seismic direction), and P3 of F3.

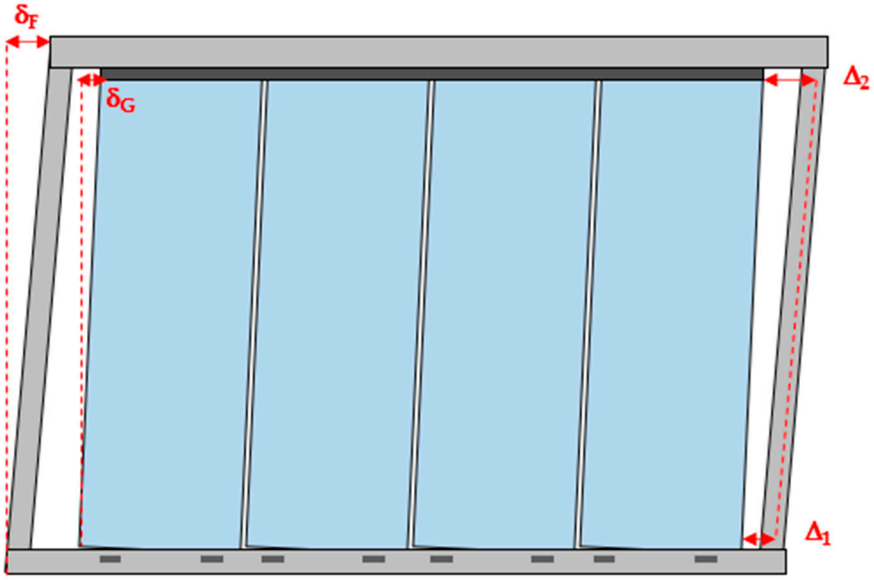

Figure 24. Scheme of the system's kinematic, highlighting the relative displacements monitored for the wall response characterisation.

A single time history (TH) analysis was selected (TH 7) to present the results in a detailed manner, while the output stemming from the whole set of ground motions was later provided using bar plots. Starting from the in-plane response of the facades F1 and F3, the outcomes are reported in Figure 25 (P1.1), Figure 26 (P1.2), and Figure 27 (P3); for each panel, three charts are provided, each showing a specific response quantity: drift δ_F in charts (a), drift δ_G in charts (b), and relative displacements Δ_1 and Δ_2 in charts (c).

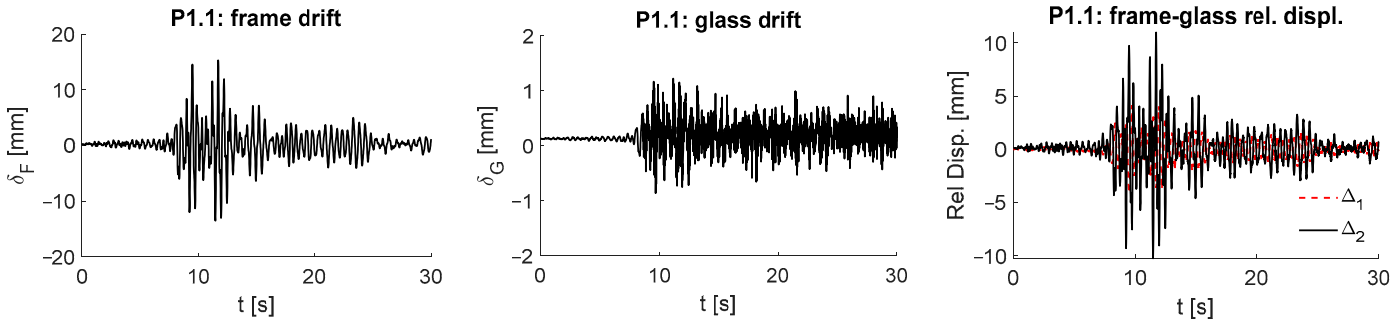

(a) (b) (c)

Figure 25. P1.1: (**a**) aluminium portal frame drift response (δ_F), (**b**) glass plate drift response (δ_G), and (**c**) relative motion (Δ_1 and Δ_2) between glass and aluminium at the top and the bottom of the wall.

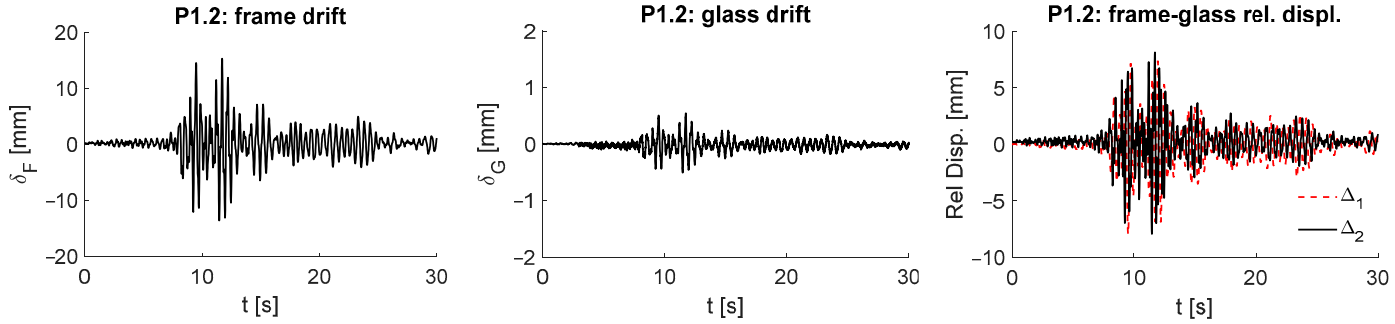

(a) (b) (c)

Figure 26. P1.2: (**a**) aluminium portal frame drift response (δ_F), (**b**) glass plate drift response (δ_G), and (**c**) relative motion (Δ_1 and Δ_2) between glass and aluminium at the top and the bottom of the wall.

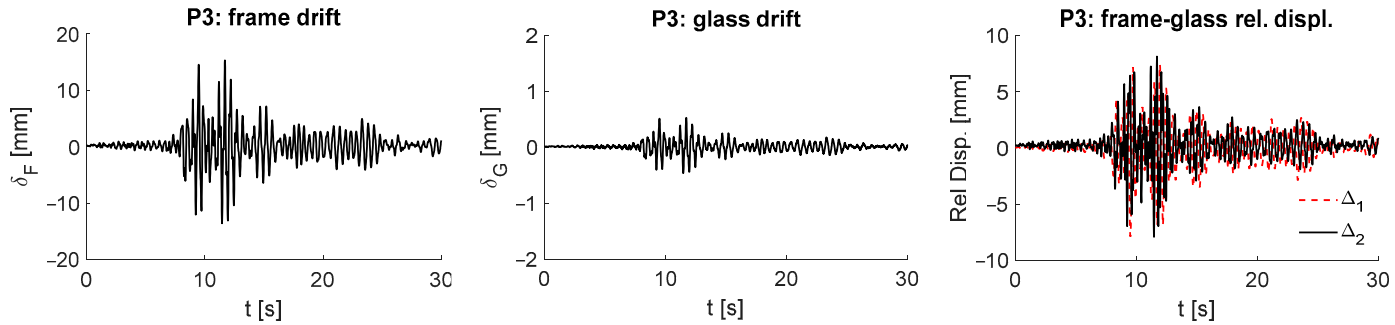

(a) (b) (c)

Figure 27. P3: (**a**) aluminium portal frame drift response (δ_F), (**b**) glass plate drift response (δ_G), and (**c**) relative motion (Δ_1 and Δ_2) between glass and aluminium at the top and the bottom of the wall.

The following comments can be made:

- The relative displacements, δ_F, experienced by the outer aluminium portal frame (Figures 25a, 26a and 27a) were the same for all the facades, as expected, and they

also corresponded to the drift experienced by the building's last storey (the maximum value, normalised by the third-storey height, attained approximately 0.55%).

- All the panels experienced relative displacements (drift) notably lower than those experienced by the floors (inter-storey drift), and this result is in line with the design objective of making the walls unsensitive to the building drift.
- The motion of the panels P1.2 and P3 appeared mainly translational, with slight rocking components (1 mm maximum) and lateral glass-aluminium relative displacements uniform and synchronous between the top and bottom.
- P1.1, due to its particular configuration, i.e., a single glass plate with a higher slenderness ratio, tended to experience a higher rocking motion (Figure 25b), thus presenting relative displacements between glass and lateral aluminium frames that were higher at the top than at the bottom (Figure 25c), which were, however, always lower than the available stroke of 25 mm (hence, glass–frame pounding was prevented).
- The residual deformations observed on the glass, due to the friction mechanisms at the base of the panels, were of the order of magnitude of a few tenths of a millimetre, and thus definitely acceptable and proof of a good recentring property of the system.

Regarding the rubber pads, in Figure 28, the force–displacement hysteretic cycles of three pairs of dissipative elements, one for each panel (P1.1, P1.2, and P3), are compared with different colours. It can be seen that the cycles of the pads belonging to panels composed by more than one glass plate were wider and more stable (hence, they had a better performance in terms of seismic energy dissipation) than those of panel P1.1, and this agrees with the earlier observation concerning the relative importance of the rocking component on the kinematic of the panel.

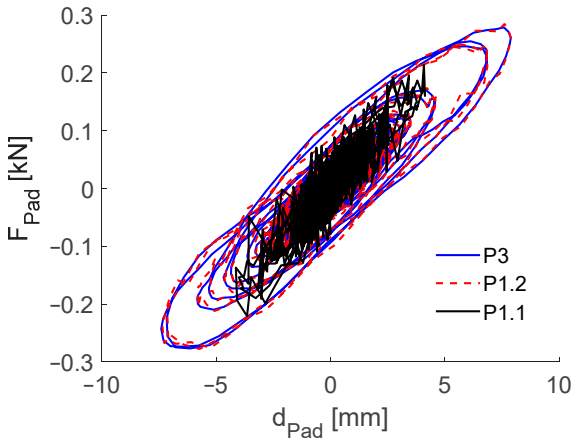

Figure 28. Rubber pads' force–displacement responses.

To complete the overview of the response of the panels oriented along the seismic direction, the charts in Figure 29 summarise, in the form of bar plots, the maximum quantities observed for the ten THs: Figure 29a shows the maxima of the relative displacements between the glass and the aluminium frame, and Figure 29b shows the maxima of the shear strains experienced by the rubber pads. From these charts, it can be concluded that:

- The clearance of 25 mm left as a safety margin against potential glass–frame pounding was adequate.
- The pads worked, on average, with a maximum shear strain around $\gamma = 1.0$, which is consistent with the design and sufficiently far from the rubber failure (experimentally observed for $\gamma > 2.0$).

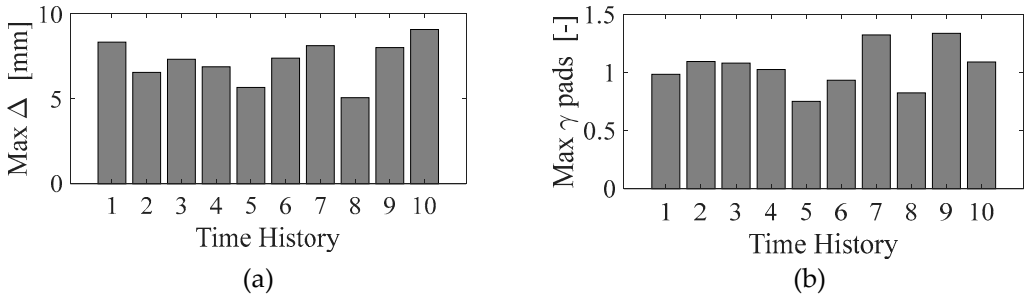

Figure 29. Maximum response quantities from all TH analyses: (**a**) relative displacements between the glass and the aluminium frame and (**b**) shear strains experienced by the rubber pads.

Finally, the response of the facade F2 was briefly analysed. In particular, due to the specific orientation of the panels, this was the only one experiencing out-of-plane actions, so the maximum stress values attained by the glass were examined and reported in Figure 30 (note that σ_{11} is the stress along the vertical direction, and σ_{22} along the transversal direction). Values were all below 30 MPa, while the minimum bending capacity of the glass is about 45 MPa for stratified glass plates, and higher than 120 MPa for tempered panels.

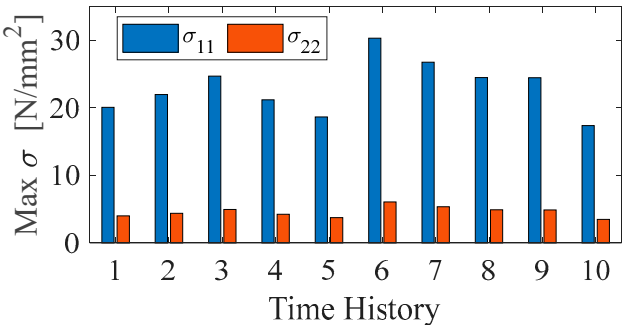

Figure 30. Maximum stresses on the glass panel subjected to out-of-plane dynamic actions.

It is also worth noting that the working rates of the aluminium profiles remained below the admissible capacity, considering that the maximum stress demands were those reported in Figure 31 and that the yielding and ultimate strength capacity values of an aluminium alloy, AW-6060 (extruded profiles with thickness lower than 5 mm), are, respectively, 120 MPa and 160 MPa [72].

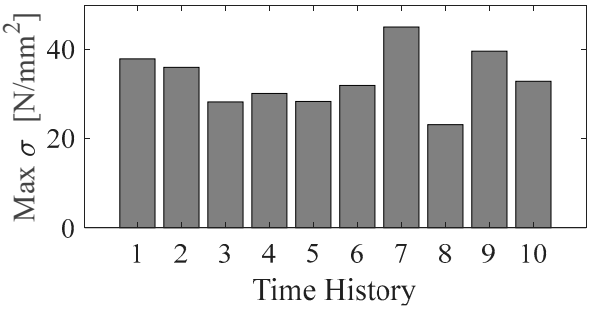

Figure 31. Maximum stresses on the aluminium frames.

To assess whether the system responses obtained from the current analyses are also representative of more complex bidirectional seismic scenarios, an orthogonal seismic component was added for case TH 7. The same horizontal input was applied simultaneously along X and Y directions. A selection of results is presented in Figure 32 for panel 3 (the right charts provide a close-up of the response time history provided on the left), and it can be seen how the responses with XY components were very similar to those stemming from

the unidirectional analysis. Deformation of the HDRPs and stresses on glass and frames were overall comparable as well, as shown in Table 3.

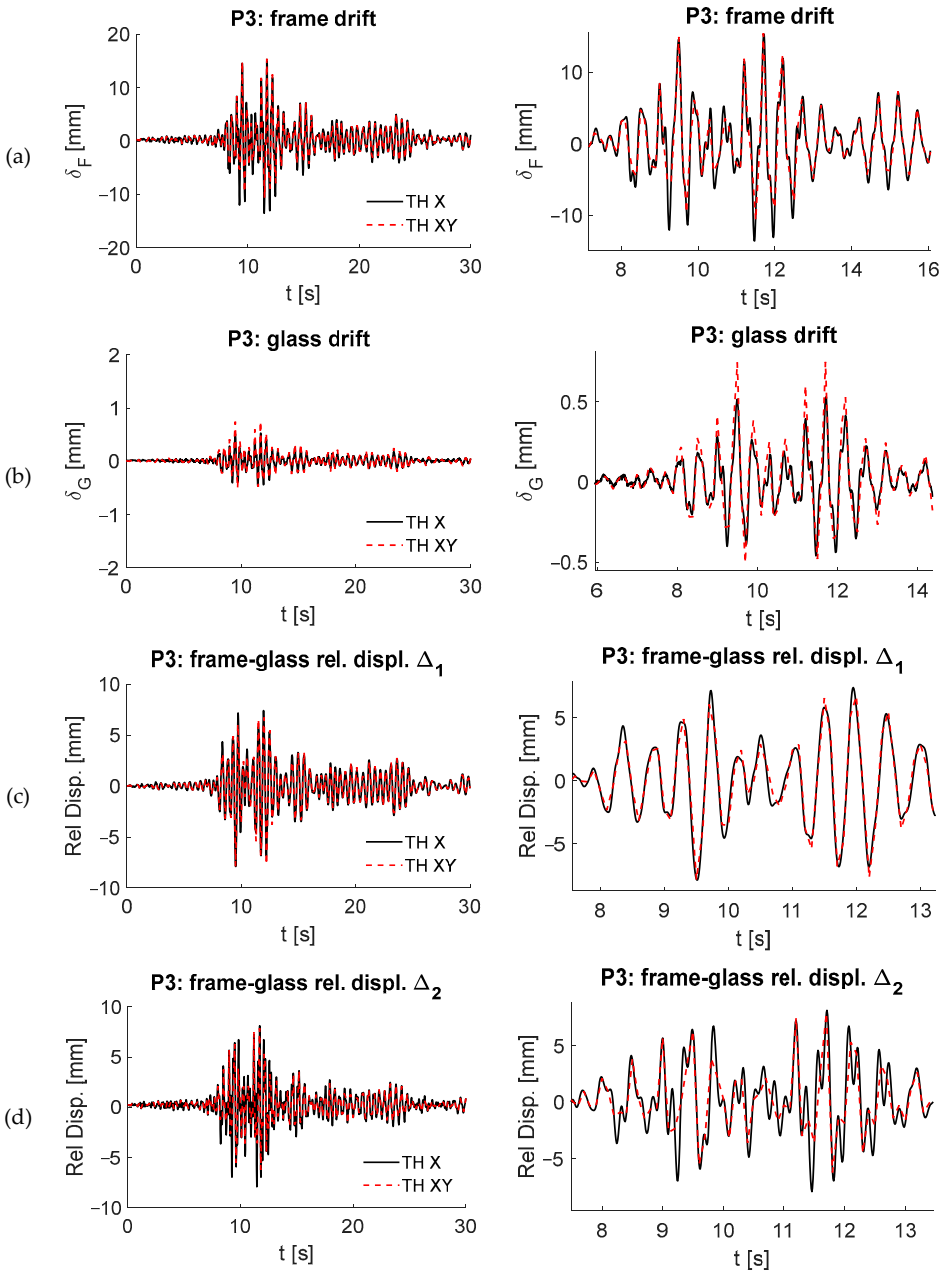

Figure 32. Response comparison (panel P3) between unidirectional and bidirectional seismic analysis: (**a**) aluminium portal frame drift response (δ_F), (**b**) glass plate drift response (δ_G), and relative motion between glass and aluminium (**c**) at the top (Δ_2) and (**d**) at the bottom (Δ_1) of the wall.

Table 3. Comparisons of unidirectional vs. bidirectional seismic responses.

Response Parameter	X Direction	XY Directions
Max. γ HDRP	1.42	1.50
Max. σ glass (MPa)	27	25
Max. σ aluminium (MPa)	30	34

5.5. Connection to the Ceiling

Numerical simulations were also performed to investigate the performance in those environments where a direct connection between the partition wall system and the upper floor was not possible, i.e., in the presence of non-structural ceilings. It was observed that by using proper spatial bracing elements (one element every 1.5 m of cladding wall length would be optimal), such as patented solutions available in the market, e.g., [73], the same seismic response, as observed for the previously analysed case of an upper direct rigid connection, could be achieved. A graphical representation of the model with this installation configuration is shown in Figure 33, while the results were not reported due to their strong similarity with those presented in the previous section.

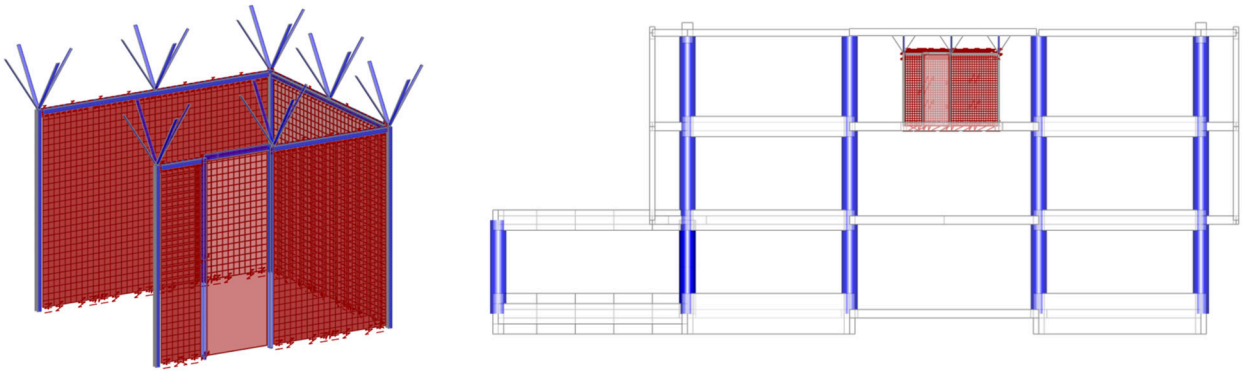

Figure 33. FEM of the system connection to the upper floor through 3D steel bracing elements (assumed and modelled as 3 mm × 40 mm steel braces with pinned connections).

5.6. Effect of the Cladding Walls on the Hosting Building

The study illustrated above confirmed the potentiality of the proposed solution and showed that the partition can dissipate the seismic input energy to withstand severe earthquakes. To complete the investigation, this section aimed at evaluating a possible beneficial contribution offered by the proposed dissipative partition wall to the hosting building. To this purpose, 72 partition walls of 3 m in length each and oriented along the X direction (24 at each floor) were placed in the model (see Figure 34) and subjected to a TH analysis with a single acceleration time series, providing as an output the temporal distribution of the most meaningful forms of energy (Figure 35), namely: seismic input energy, modal damping energy (5% constant damping), and energy dissipated by the walls. The structure was elastic.

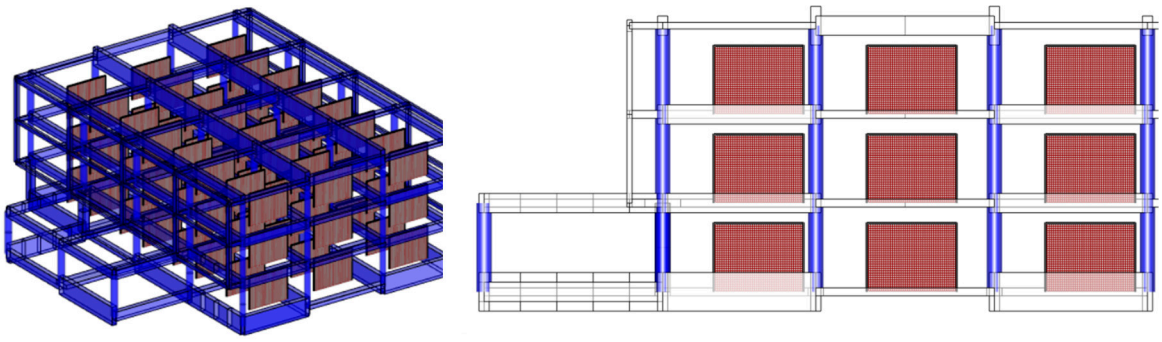

Figure 34. FEM of the building with 72 partition walls installed.

As expected, the damping contribution of the dissipative partition walls was small, but not negligible: it was about 4% of the global energy balance. Accordingly, the proposed solution cannot be considered an effective seismic passive protection for the building, despite that there is a margin for increasing its dissipation capacity, for instance, making

the rubber pads slightly shorter, thus, allowing higher displacements. Clearance between the glass and the portal frame was indeed sufficiently high to accommodate relative displacements of up to 25 mm, while the current design exploited only 10 mm.

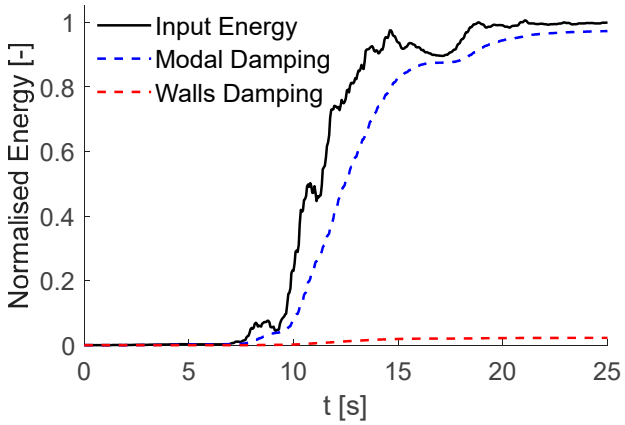

Figure 35. Normalised energy temporal distribution, highlighting the main sources of energy dissipation.

6. Conclusions

An innovative solution for aluminium-glass partition walls was developed with the aim of avoiding in-plane damage during seismic events. Such goal was achieved through a redesign of the aluminium frames used in commercially available products, allowing in-plane motion of the glass panels that activates the shear deformation of high-damping rubber pads (HDRPs) interposed between the glass panels and the aluminium frame installed at the floor.

A detailed presentation of the system conception was illustrated, showing the main intermediate steps that led to the final solution, to clearly understand the role of each component and the reasons behind their shapes. The implementation of a finite element model and its calibration based on a set of experimental tests previously performed on materials and subcomponents was then presented. Finally, a numerical application to a realistic case study consisting of a partition wall system within a three-storey building was illustrated.

Results indicated that the proposed solution was effective as a viable innovation permitting aluminium-glass partition walls to accommodate inter-storey drift, such as that experienced during severe earthquakes, with displacement mechanisms that were compatible with their geometry and with stress levels in the materials that were well below safety values. In addition, extra clearance was allowed for larger-than-expected horizontal movements as well as unexpected deformations in the aluminium frame induced by the damage of structural elements to which the partition wall was attached, reducing the risk of possible locking in the glass panel movement.

It is worth mentioning that the possibility to choose the number of pads for each glass panel made the system easily adaptable to the seismic hazard conditions and/or to different positions, e.g., lower or higher floor levels, within the building in which the partition wall was installed. If industrialised, specifications could be given to the end user by the partition supplier on the number and position of the HDRPs in relation to the seismic hazard of the site, the typology of the hosting building, and the floor level at which the partition will be installed.

Author Contributions: Conceptualisation, F.S., A.Z. and A.D.; data curation, F.S. and A.Z.; formal analysis, F.S.; investigation, F.S. and A.Z.; methodology, F.S. and A.Z.; project administration, A.D.; resources, A.D.; software, F.S.; supervision, A.Z.; validation, F.S.; visualisation, F.S.; writing—original draft, F.S. and A.Z.; writing—review and editing, F.S., A.Z. and A.D. All authors have read and agreed to the published version of the manuscript.

Funding: This work has been partially supported by the European Union—Next Generation EU—National Recovery and Resilience Plan, Mission 4 Education and Research—Component 2 From Research to Business—Investment 1.5, ECS_00000041-VITALITY—Innovation, Digitalisation and Sustainability for the Diffused Economy in Central Italy, CUP J13C22000430001. Funding of the initial research development (2018–2021) was provided by the Italian Ministry of University and Research, PON Research and Innovation, "Design, Creativity and Made in Italy" specialisation area, project "S.A.F.E. Sustainable Design of Anti-Seismic Furniture as Smart Life-Saving Systems during an Earthquake".

Data Availability Statement: Data are available upon reasonable request from the corresponding author.

Acknowledgments: The authors acknowledge the economic support provided by the Italian Ministry of University and Research and by the European Commission. The authors acknowledge the constructive interactions with the industrial design research team (Lucia Pietroni, Jacopo Mascitti, and colleagues) at the University of Camerino and with the industrial partner Styloffice S.p.A. (Miglianico, Italy) during the design and prototyping stages, the support of Hamid Ahmadi at Rubber Consultants (London, UK) in defining the high-damping rubber compound, and the valuable collaboration with Felice Carlo Ponzo and his structural engineering research team at the University of Basilicata (Potenza, Italy) while designing the experimental testing described in other coauthored publications.

Conflicts of Interest: The authors declare no conflicts of interest.

References

1. Villaverde, R. Seismic Analysis and Design of Nonstructural Elements. In *Earthquake Engineering: From Engineering Seismology to Performance-Based Engineering*; Bozorgnia, Y., Bertero, V., Eds.; CRC Press: Boca Raton, FL, USA, 2004.
2. Hashemi, A.; Mosalam, K.M. Shake-table experiment on reinforced concrete structure containing masonry infill wall. *Earthq. Eng. Struct. Dyn.* **2006**, *35*, 1827–1852. [CrossRef]
3. Dolšek, M.; Fajfar, P. The effect of masonry infills on the seismic response of a four-storey reinforced concrete frame—A deterministic assessment. *Eng. Struct.* **2008**, *30*, 1991–2001. [CrossRef]
4. Stavridis, A.; Koutromanos, I.; Shing, P.B. Shake-table tests of a three-story reinforced concrete frame with masonry infill walls. *Earthq. Eng. Struct. Dyn.* **2012**, *41*, 1089–1108. [CrossRef]
5. Uva, G.; Porco, F.; Fiore, A. Appraisal of masonry infill walls effect in the seismic response of RC framed buildings: A case study. *Eng. Struct.* **2012**, *34*, 514–526. [CrossRef]
6. De Luca, F.; Verderame, G.M.; Gómez-Martínez, F.; Pérez-García, A. The structural role played by masonry infills on RC building performances after the 2011 Lorca, Spain, earthquake. *Bull. Earthq. Eng.* **2014**, *12*, 1999–2026. [CrossRef]
7. Ricci, P.; Di Domenico, M.; Verderame, G.M. Experimental assessment of the in-plane/out-of-plane interaction in unreinforced masonry infill walls. *Eng. Struct.* **2018**, *173*, 960–978. [CrossRef]
8. De Matteis, G.; Landolfo, L.; Mazzolani, F.M. Diaphragm effect for industrial steel buildings under earthquake loading. *J. Constr. Steel Res.* **1998**, *46*, 357–358. [CrossRef]
9. De Matteis, G. Effect of lightweight cladding panels on the seismic performance of moment resisting steel frames. *Eng. Struct.* **2005**, *27*, 1662–1676. [CrossRef]
10. Okazaki, T.; Nakashima, M.; Suita, K.; Matusmiya, T. Interaction between cladding and structural frame observed in a full-scale steel building test. *Earthq. Eng.Struct. Dyn.* **2007**, *36*, 35–53. [CrossRef]
11. Mastrogiuseppe, S.; Rogers, C.A.; Tremblay, R.; Nedisan, C.D. Influence of nonstructural components on roof diaphragm stiffness and fundamental periods of single-storey steel buildings. *J. Constr. Steel Res.* **2008**, *64*, 214–227. [CrossRef]
12. Scozzese, F.; Terracciano, G.; Zona, A.; Della Corte, G.; Dall'Asta, A.; Landolfo, R. Analysis of seismic non-structural damage in single-storey industrial steel buildings. *Soil Dyn. Earthq. Eng.* **2018**, *114*, 505–519. [CrossRef]
13. Dhakal, R.P. Damage to non-structural components and contents in 2010 darfield earthquake. *Bull. N. Z. Soc. Earthq. Eng.* **2010**, *43*, 404–410. [CrossRef]
14. Taghavi, S.; Miranda, E. *Response Assessment of Nonstructural Building Elements. Report 2003/05*; Pacific Earthquake Engineering Research (PEER) Centre: Berkley, CA, USA, 2003; p. 96.
15. Khakurel, S.; Dhakal, R.P.; Yeow, T.; Saha, S. Performance group weighting factors for rapid seismic loss estimation of buildings of different usage. *Earthq. Spectra.* **2020**, *36*, 1141–1165. [CrossRef]
16. Bradley, B.A.; Dhakal, R.P.; Cubrinovski, M.; MacRae, G.A. Seismic loss estimation for efficient decision making. *Bull. N. Z. Soc. Earthq. Eng.* **2009**, *42*, 96–110. [CrossRef]
17. Dhakal, R.P.; Pourali, A.; Saha, S. Simplified seismic loss functions for suspended ceilings and drywall partitions. *Bull. N. Z. Soc. Earthq. Eng.* **2016**, *49*, 64–78. [CrossRef]
18. Sousa, L.; Monteiro, R. Seismic retrofit options for non-structural building partition walls: Impact on loss estimation and cost-benefit analysis. *Eng. Struct.* **2018**, *161*, 8–27. [CrossRef]

19. Takagi, J.; Wada, A. Recent earthquakes and the need for a new philosophy for earthquake-resistant design. *Soil Dyn. Earthq. Eng.* **2019**, *119*, 499–507. [CrossRef]
20. Arifin, F.A.; Sullivan, T.J.; MacRae, G.; Kurata, M.; Takeda, T. Lessons for loss assessment from the Canterbury earthquakes: A 22-storey building. *Bull. Earthq. Eng.* **2021**, *19*, 2081–2104. [CrossRef]
21. O'Reilly, G.J.; Hasegawa, K.; Shahnazaryan, D.; Poveda, J.; Fukutomi, Y.; Kusaka, A.; Nakashima, M. On the fragility of non-structural elements in loss and recovery: Field observations from Japan. *Earthq. Eng. Struct. Dyn.* **2024**, *53*, 1125–1144. [CrossRef]
22. Ahmad, Z.; Ahmed, H.A.; Shahzada, K.; Li, Y. Vulnerability of Non-Structural Elements (NSEs) in Buildings and Their Life Cycle Assessment: A Review. *Buildings* **2024**, *14*, 170. [CrossRef]
23. Preti, M.; Bettini, N.; Migliorati, L.; Bolis, V.; Stavridis, A.; Plizzari, G.A. Analysis of the in-plane response of earthen masonry infill panels partitioned by sliding joints. *Earthq. Eng. Struct. Dyn.* **2016**, *45*, 1209–1232. [CrossRef]
24. Palios, X.; Fardis, M.N.; Strepelias, E.; Bousias, S.N. Unbonded brickwork for the protection of infills from seismic damage. *Eng. Struct.* **2017**, *131*, 614–624. [CrossRef]
25. Tsantilis, A.V.; Triantafillou, T.C. Innovative seismic isolation of masonry infills using cellular materials at the interface with the surrounding RC frames. *Eng. Struct.* **2018**, *155*, 279–297. [CrossRef]
26. Marinković, M.; Butenweg, C. Innovative decoupling system for the seismic protection of masonry infill walls in reinforced concrete frames. *Eng. Struct.* **2019**, *197*, 09435. [CrossRef]
27. Dhir, P.K.; Tubaldi, E.; Ahmadi, H.; Gough, J. Numerical modelling of reinforced concrete frames with masonry infills and rubber joints. *Eng. Struct.* **2021**, *246*, 112833. [CrossRef]
28. Dhir, P.K.; Tubaldi, E.; Panto, B.; Calio, I. A macro-model for describing the in-plane seismic response of masonry-infilled frames with sliding/flexible joints. *Earthq. Eng.Struct. Dyn.* **2022**, *51*, 3022–3044. [CrossRef]
29. Lee, T.H.; Kato, M.; Matsumiya, T.; Suita, K.; Nakashima, M. Seismic performance evaluation of non-structural components: Drywall partitions. *Earthq. Eng. Struct. Dyn.* **2007**, *36*, 367–382. [CrossRef]
30. Restrepo, J.I.; Bersofsky, A.M. Performance characteristics of light gage steel stud partition walls. *Thin-Walled Struct.* **2011**, *49*, 317–324. [CrossRef]
31. Retamales, R.; Davies, R.; Mosqueda, G.; Filiatrault, A. Experimental seismic fragility of cold-formed steel framed gypsum partition walls. *J. Struct. Eng.* **2013**, *139*, 1285–1293. [CrossRef]
32. Magliulo, G.; Petrone, C.; Capozzi, V.; Maddaloni, G.; Lopez, P.; Manfredi, G. Seismic performance evaluation of plasterboard partitions via shake table tests. *Bull. Earthq. Eng.* **2013**, *12*, 1657–1677. [CrossRef]
33. Tasligedik, A.S.; Pampanin, S.; Palermo, A. Low damage seismic solutions for non-structural drywall artitions. *Bull. Earthq. Eng.* **2014**, *13*, 1029–1050. [CrossRef]
34. Wang, X.; Pantoli, E.; Hutchinson, T.C.; Restrepo, J.I.; Wood, R.L.; Hoehler, M.S.; Grzesik, P.; Sesma, F.H. Seismic performance of cold-formed steel wall systems in a full-scale building. *J. Struct. Eng.* **2015**, *141*, 04015014. [CrossRef]
35. Rahmanishamsi, E.; Soroushian, S.; Maragakis, E. Analytical model for the in-plane seismic performance of cold-formed steel-framed gypsum partition walls. *Earthq. Eng. Struct. Dyn.* **2015**, *45*, 619–634. [CrossRef]
36. Petrone, C.; Magliulo, G.; Lopez, P.; Manfredi, G. Seismic fragility of plasterboard partitions via in-plane quasi-static tests. *Earthq. Eng. Struct. Dyn.* **2015**, *44*, 2589–2606. [CrossRef]
37. Petrone, C.; Magliulo, G.; Lopez, P.; Manfredi, G. Out-of-plane seismic performance of plasterboard partitions via quasi-static tests. *Bull. N. Z. Soc. Earthq. Eng.* **2016**, *49*, 125–137. [CrossRef]
38. Jenkins, C.; Soroushian, S.; Rahmanishamsi, E.; Maragakis, E.M. Experimental fragility analysis of cold-formed steel-framed partition wall systems. *Thin-Walled Struct.* **2016**, *103*, 115–127. [CrossRef]
39. Rahmanishamsi, E.; Soroushian, S.; Maragakis, E.M. Cyclic shear behavior of gypsum board-to-steel stud screw connections in nonstructural walls. *Earthq. Spectra.* **2016**, *32*, 415–439. [CrossRef]
40. Rahmanishamsi, E.; Soroushian, S.; Maragakis, E.M. Evaluation of the out-of-plane behavior of stud-to-track connections in nonstructural partition walls. *Thin-Walled Struct.* **2016**, *103*, 211–224. [CrossRef]
41. Rahmanishamsi, E.; Soroushian, S.; Maragakis, E.M. Analytical model to capture the in-plane and out-of-plane seismic behavior of nonstructural partition walls with returns. *J. Struct. Eng.* **2017**, *143*, 6. [CrossRef]
42. Petrone, C.; Magliulo, G.; Manfredi, G. Shake table tests on standard and innovative temporary partition walls. *Earthq. Eng. Struct. Dyn.* **2017**, *46*, 1599–1624. [CrossRef]
43. Petrone, C.; Coppola, O.; Magliulo, G.; Lopez, P.; Manfredi, G. Numerical model for the in-plane seismic capacity evaluation of tall plasterboard internal partitions. *Thin-Walled Struct.* **2018**, *122*, 572–584. [CrossRef]
44. Fiorino, L.; Pali, T.; Landolfo, R. Out-of-plane seismic design by testing of non-structural lightweight steel drywall partition walls. *Thin-Walled Struct.* **2018**, *130*, 213–230. [CrossRef]
45. Pali, T.; Macillo, V.; Terracciano, M.T.; Bucciero, B.; Fiorino, L.; Landolfo, R. In-plane quasi-static cyclic tests of nonstructural lightweight steel drywall partitions for seismic performance evaluation. *Earthq. Eng. Struct. Dyn.* **2018**, *47*, 1566–1588. [CrossRef]
46. Fiorino, L.; Bucciero, B.; Landolfo, R. Evaluation of seismic dynamic behaviour of drywall partitions, façades and ceilings through shake table testing. *Eng. Struct.* **2019**, *180*, 103–123. [CrossRef]
47. Araya-Letelier, G.; Miranda, E.; Deierlein, G. Development and Testing of a Friction/Sliding Connection to Improve the Seismic Performance of Gypsum Partition Walls. *Earthq. Spectra.* **2019**, *35*, 653–677. [CrossRef]

48. Mulligan, J.; Sullivan, T.; Dhakal, R. Experimental Seismic Performance of Partly-Sliding Partition Walls. *J. Earthq. Eng.* **2020**, *26*, 1630–1655. [CrossRef]
49. Mulligan, J.; Sullivan, T.; Dhakal, R. Experimental study of the seismic performance of plasterboard partition walls with seismic gaps. *Bull. N. Z. Soc. Earthq. Eng.* **2020**, *53*, 175–188. [CrossRef]
50. Salmasi Javid, H.; Soroushian, S.; Rahmanishamsi, E.; Maragakis, E.M. Methodology for the Development of Analytical Seismic Fragility for Full Connection Steel-Framed Gypsum Partition Walls. *J. Earthq. Eng.* **2020**, *26*, 4129–4146. [CrossRef]
51. Shin, D.-H.; Kim, H.-J. Macro-modelling approach for the in-plane cyclic response of cold-formed steel partition walls. *Appl. Sci.* **2020**, *10*, 8163. [CrossRef]
52. Kim, H.J.; Shin, D.H. Shake table test program of cold-formed steel in-plane partition walls. *Structures* **2021**, *30*, 503–517. [CrossRef]
53. Wang, D.; Zhi, X.; Zhu, F.; Wang, Y. Seismic Fragility of Chinese Light-Gauge Steel Keel Gypsum Board Partition Walls. *Shock. Vib.* **2021**, *2021*, 8875486. [CrossRef]
54. Lotfy, I.; Salkhordeh, M.; Soroushian, S.; Rahmanishamsi, E.; Maragakis, E.M. Development of the simplified spring-based nonlinear models for full-connection cold-formed steel-framed gypsum partition walls. *Earthq. Eng. Struct. Dyn.* **2023**, *52*, 1317–1338. [CrossRef]
55. Huang, J.; Kurata, M.; Shen, S.-D. Experimental investigation and modeling of boundary influences on in-plane seismic performance of partition walls. *Earthq. Eng. Struct. Dyn.* **2024**, *53*, 924–942. [CrossRef]
56. Huang, J.; Kurata, M.; Kawamata, Y.; Kanao, I.; Qi, L.; Takaoka, M. In-Plane damage of partition walls with various boundaries during earthquakes. *Earthq. Eng. Struct. Dyn.* **2023**, *52*, 1059–1077. [CrossRef]
57. Ditommaso, R.; Scozzese, F.; Mossucca, A.; Auletta, G.; Di Cesare, A.; Nigro, D.; Zona, A.; Ponzo, F.C.; Dall'Asta, A. Preliminary results in the design and testing of earthquake-proof glass-aluminium partition walls. In Proceeding of the 17th World Conference on Seismic Isolation ASSISI, Turin, Italy, 12–15 September 2022. [CrossRef]
58. Scozzese, F.; Ditommaso, R.; Zona, A.; Ponzo, F.C.; Di Cesare, A.; Dall'Asta, A. Earthquake-proof glass-aluminium partition walls with viscoelastic dissipative devices. In Proceeding of the 18th World Conference on Earthquake Engineering (WCEE2024), Milan, Italy, 30 June–5 July 2024.
59. Payne, A.R. The dynamic properties of carbon black-loaded natural rubber vulcanizates. Part, I. *J. Appl. Polym. Sci.* **1962**, *6*, 57–63. [CrossRef]
60. Lion, A. A constitutive model for carbon black filled rubber: Experimental investigation and mathematical representation. *Contin. Mech. Thermodyn.* **1996**, *8*, 153–169. [CrossRef]
61. Tubaldi, E.; Ragni, L.; Dall'Asta, A.; Ahmadi, H.; Muhr, A. Stress softening behaviour of HDNR bearings: Modelling and influence on the seismic response of isolated structures. *Earthq. Eng. Struct. Dyn.* **2017**, *46*, 2033–2054. [CrossRef]
62. Micozzi, F.; Scozzese, F.; Ragni, L.; Dall'Asta, A. Seismic reliability of base isolated systems: Sensitivity to design choices. *Eng. Struct.* **2022**, *256*, 114056. [CrossRef]
63. Xian, W.; Zhan, Y.-S.; Maiti, A.; Saab, A.P.; Li, Y. Filled Elastomers: Mechanistic and Physics-Driven Modeling and Applications as Smart Materials. *Polymers* **2024**, *16*, 1387. [CrossRef]
64. Xu, Z.D.; Xu, C.; Hu, J. Equivalent fractional Kelvin model and experimental study on viscoelastic damper. *J. Vib. Control* **2015**, *21*, 2536–2552. [CrossRef]
65. Xu, Z.D.; Liao, Y.X.; Ge, T.; Xu, C. Experimental and theoretical study of viscoelastic dampers with different matrix rubbers. *J. Eng. Mech.* **2016**, *142*, 04016051. [CrossRef]
66. Xu, Z.D.; Ge, T.; Liu, J. Experimental and theoretical study of high-energy dissipation-viscoelastic dampers based on acrylate-rubber matrix. *J. Eng. Mech.* **2020**, *146*, 04020057. [CrossRef]
67. Dall'Asta, A.; Ragni, L. Experimental Tests and Analytical Model of High Damping Rubber Dissipating Devices. *Eng. Struct.* **2006**, *28*, 1874–1884. [CrossRef]
68. *SAP2000*, Ultimate Version 25.3.0.; Integrated Finite Element Analysis and Design of Structures; Computers and Structures Inc.: Berkeley, CA, USA, 2024.
69. Dall'Asta, A.; Ragni, L. Dynamic systems with high damping rubber: Nonlinear behaviour and linear approximation. *Earthq. Eng. Struct. Dyn.* **2008**, *37*, 1511–1526. [CrossRef]
70. Micozzi, F.; Ragni, L.; Gioiella, L.; Quaglini, V.; Dall'Asta, A. Variability of Dynamic Properties of Rubber Compounds for Elastomeric Bearings. *Struct. Control. Health Monit.* **2023**, *1*, 6638748. [CrossRef]
71. Federal Emergency Management Agency (FEMA). *NEHRP Commentary on the Guidelines for the Seismic Rehabilitation of Buildings, FEMA Publication 274*; Federal Emergency Management Agency: Washington, DC, USA, 1997.
72. Mazzolani, F. *Aluminium Alloy Structures*, 2nd ed.; CRC Press: Boca Raton, FL, USA, 2019.
73. Brandolese, S.; Fiorin, L.; Scotta, R. Seismic demand and capacity assessment of suspended ceiling systems. *Eng. Struct.* **2019**, *193*, 219–237. [CrossRef]